frontiers | Frontiers in Forests and Global Change

TYPE Original Research
PUBLISHED 03 March 2026
DOI 10.3389/ffgc.2025.1707812

OPEN ACCESS

EDITED BY
David Ellison,
Swedish University of Agricultural Sciences, Sweden

REVIEWED BY
Ravindra Dwivedi,
University of Arizona, United States
Wyatt Reis,
Cold Regions Research and Engineering Laboratory, United States

*CORRESPONDENCE
Cassie Lumbrazo
✉ cassielumbrazo@gmail.com

RECEIVED 17 September 2025
REVISED 11 November 2025
ACCEPTED 03 December 2025
PUBLISHED 03 March 2026

CITATION
Lumbrazo C, Howe ER, Dickerson-Lange SE, Pestana S, Cramblitt J, Dedinsky K, Smith K and Lundquist JD (2026) Can we maximize snow storage through fire-resilient forest treatments? Insights from experimental forest treatments in the Eastern Cascades, WA, USA.
Front. For. Glob. Change 8:1707812.
doi: 10.3389/ffgc.2025.1707812

Can we maximize snow storage through fire-resilient forest treatments? Insights from experimental forest treatments in the Eastern Cascades, WA, USA

Cassie Lumbrazo[1,2]*, Emily R. Howe[3], Susan E. Dickerson-Lange[4], Steven Pestana[1], John Cramblitt[1,5], Karen Dedinsky[1], Kyle Smith[3] and Jessica D. Lundquist[1]

[1]Department of Civil and Environmental Engineering, University of Washington, Seattle, WA, United States, [2]Department of Natural Sciences, University of Alaska Southeast, Juneau, AK, United States, [3]The Nature Conservancy of Washington, Seattle, WA, United States, [4]Climate Impacts Group, University of Washington, Seattle, WA, United States, [5]Department of Geography, University of California, Berkeley, CA, United States

Forest treatments such as prescribed burns, mastication, and thinning are widely implemented across the western USA to reduce fuels and enhance wildfire resilience. These practices also influence snow accumulation and melt, which, in turn, affect snow storage and duration. Since many regions depend on seasonal snow for water resources, it is essential that forest management practices preserve or even enhance snow storage as a buffer against the impacts of climate change. To test the hypothesis that thinning and canopy gap creation can maximize snow storage, particularly on north-facing slopes, experimental forest treatments representing a range of thinning intensities were implemented on Cle Elum Ridge in the headwaters of the Yakima River Basin, Washington, USA. Ground-based snow observations, combined with pre-treatment (2021) and post-treatment (2023) snow-on lidar, show that canopy thinning increased snow depth and storage by 30% on north-facing slopes and by 16% on south-facing slopes. Snow depth was positively related to canopy openness, as measured by sky view fraction and canopy edge metrics, with stronger effects on north-facing slopes. In contrast, there was no clear relationship between snow depth and degree of thinning as measured by forest basal area, a common forestry metric used to plan treatment prescriptions. Using canopy edge metrics and sky view fraction relationships, we estimated the hydrologic benefit of thinning during 2023 at 12.3 acre-feet of water storage per 100 acres of north-facing forest and 5.1 acre-feet on south-facing slopes. These findings highlight the potential to incorporate hydrologic resilience as a co-benefit when planning fuel reduction strategies.

KEYWORDS

forest management, snow, wildfire, water resources, forest thinning, canopy gaps, snow water equivalent

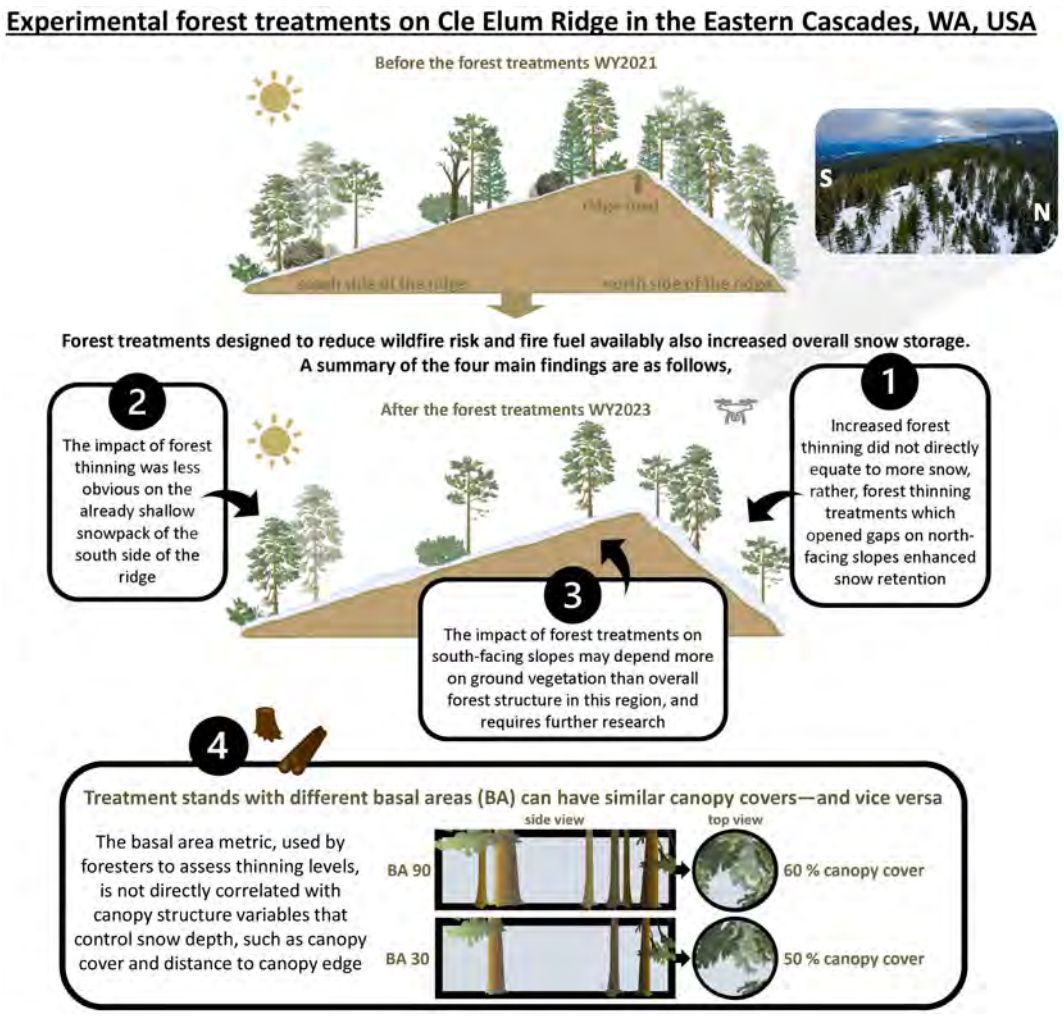

GRAPHICAL ABSTRACT
This graphic abstract includes adapted illustrations from the Integration and Application Network, University of Maryland Center for Environmental Science (ian.umces.edu/media-library), used under CC BY-SA 4.0. Full attribution provided is in the Acknowledgments.

Highlights

- Forest treatments to reduce wildfire risk also increased snow storage at this site.
- Treatments on north-facing slopes enhanced snow depth more than on south-facing slopes.
- Canopy cover predicts snow depth and snow retention better than basal area.
- Small to mid-sized canopy gaps had more snow storage than closed canopy sites.
- The role of ground cover on snow depth in south-facing slopes needs further research.

1 Introduction

1.1 Forest-snow interactions and management

Water scarcity is a pressing social-ecological issue across the western United States of America (USA) that poses significant adaptation challenges for both people and nature. Together, increasing per capita water consumption and climate change will reduce water supplies and increase demand in many regions, leading to severe water shortages (Brown et al., 2019). In many western USA basins, seasonal snowpack is an essential ecohydrological component of total water supply, supporting 53–78% of the surface water used in municipal, agricultural, and industrial systems (Koshkin et al., 2022; Li et al., 2017; Pierce et al., 2008). Snowpack also supports key ecological processes related to forest growth, plant phenology, soil water stress, and wildfire activity (Sanmiguel-Vallelado et al., 2022). It drives hydrological flows and thermal regimes that are critical to aquatic species (Cline et al., 2020). However, seasonal snowpack has declined over the last century due to a warming climate (Mote et al., 2005, 2018), and these losses are projected to continue (Musselman et al., 2017, 2018). For example, the snowpack in the Cascades Range of Washington State is projected to decrease by 50% over the next 70 years (Duan et al., 2017; Li et al., 2017).

In addition to reducing water storage and availability, decreasing snowpack—especially spring mountain snowpack—contributes to declines in summer soil moisture and fuel moisture (Gergel et al., 2017). In turn, low moisture levels increase the potential for larger and

more intense wildfires, particularly in montane regions where biomass fuel is abundant and vapor pressure deficit is rising (Abatzoglou and Williams, 2016; Gergel et al., 2017). Across the western USA, climate-fire models project a doubling of forest-fire areas between 2021 and 2050 compared to 1990–2020 (Abatzoglou et al., 2021). A growing wildfire area is underpinned by several anthropogenic factors that have shifted forest structure and vulnerability over time, including historically high fuel loads due to a century of fire suppression, the outlawing of Indigenous cultural burning, the selective logging of the oldest, and the majority of fire-resistant trees, and increased fuel dryness resulting from human-caused climate change (Abatzoglou et al., 2018; Hagmann et al., 2021).

Of particular concern, however, is the finding that the geographical overlap between fire and the seasonal snow zone is accelerating in the American West, with the total burned area within the seasonal snow zone increasing at a rate of 9% per year since 1984 (Gleason et al., 2019). Given that positive feedback loops between wildfire and snowpack can increase melt rates by 57% and shorten snowpack duration by 4 to 23 days, increasing wildfires within the seasonal snow zone diminish the function of mountain snowpacks to store water (Gleason et al., 2019; Koshkin et al., 2022). Thus, increasing wildfires can reduce water storage and worsen summer drought conditions.

Although resource managers are unlikely to affect the total burn area each year, implementing spatially strategic fuel treatments at landscape scales can help reduce wildfire intensity and severity, protecting communities and improving forest resilience to fire, insects, and drought (Halofsky et al., 2020). In the western USA, active forest management aimed at preventing catastrophic wildfire includes a combination of mechanical thinning and mastication to reduce forest density and fuel loads, followed by prescribed or Indigenous cultural burns to reduce understory fuels, create diverse forest mosaics, and support culturally significant species (Churchill et al., 2013; Everett et al., 2000; Prichard et al., 2021). These adaptation measures are increasingly being adopted by natural resource agencies, with the United States federal government having recently (2021) injected $3.3 billion into wildfire mitigation, forest management, and community preparedness over the next 10 years (Weinberger, 2022).

While thinning and prescribed burns are being implemented across the western USA to reduce wildfire hazards, increase forest resilience, and improve forest health, less attention has been given to their impact on hydrologic resilience. Following Newton and Spence (2023), we define hydrologic resilience as the ability of a watershed to maintain hydrological function within historical bounds. Similar to fire behavior, snowpack dynamics are strongly mediated by a complex set of interactions between meteorological conditions, topography, and vegetation structure, with the presence and structure of forest canopies affecting both the amount and duration of snow storage on the landscape (Dickerson-Lange et al., 2017, 2021; Lundquist et al., 2013; Sanmiguel-Vallelado et al., 2022). The overall effect of forests on snow storage and duration varies significantly across regional scales, ranging from snow persisting several weeks longer in forest gaps (Bales et al., 2011; Dickerson-Lange et al., 2015; Storck, 2000), where more snow accumulates due to lack of canopy-snow interception, to 2 weeks longer under forest canopy (Gelfan et al., 2004; Koivusalo and Kokkonen, 2002; Rutter et al., 2009), where ablation rates may be diminished due to shading and wind protection (Manning et al., 2025). This implies that forest management effects on hydrologic resilience will not be uniform across broad geographic scales, and effective management strategies will require location-specific empirical evidence or modeling.

While topographic features and regional climate are considered 'fixed' from a management perspective, processes related to forest structure can be modified to influence hydrologic processes, offering an opportunity for adaptive management actions that buffer against climate change (Churchill et al., 2013; Dickerson-Lange et al., 2023). In this study, we explore the management intersection between wildfire resilience and hydrologic resilience by focusing on forest canopy-snow interactions across a gradient of forest densities in the Eastern Cascade Mountain Range in Washington State, USA. This intersection has been generally identified as a key data gap for improving parameterizations in models used to evaluate forest impacts on water resources (Koshkin et al., 2022). Furthermore, the specific geographic area we investigate represents a challenging-to-model transitional climate zone between warm and wet maritime conditions and cold and dry continental conditions, a relative spatial data gap for observational forest-snow data (Dickerson-Lange et al., 2023), a priority area for wildfire resilience projects (Washington State Department of Natural Resources, 2018b), and the headwaters of a climate-vulnerable snowpack-dependent watershed (Donley et al., 2012).

1.2 Research goals

Our two research goals include (1) identifying whether forest thinning prescriptions for fire resilience exacerbate climate stressors on hydrologic resilience or whether these prescriptions promote hydrologic resilience and (2) producing guidance directly applicable to forest managers in the region. Therefore, we co-developed our research questions with the Tapash Sustainable Forest Collaborative to ask the following: (1) how do forest thinning approaches designed to reduce wildfire severity affect the amount and duration of snow storage on the landscape? (2) what level of forest thinning most effectively promotes snow storage across north- versus south-facing slopes?

To answer these questions, we combine 2 years of on the ground and remotely sensed observations to quantify snow storage responses to a gradient of forest density in a dry-forest ecosystem near Cle Elum, Washington, USA. We specifically investigate:

1. What is the snow depth response to a gradient of forest densities as a function of slope aspect?
   a. At the plot scale (exactly 10 m x 10 m; ~0.02 acres), defined by field-measured basal area?
   b. At the stand scale (typically 0.08–4 hectares; 0.2–10 acres), defined by field-delineated forest treatment stands and by lidar-defined forest treated areas?
2. What is the snow depth response to the overall forest structure across the site by aspect?
3. How does total snow storage (calculated as snow water equivalent; SWE) change before and after forest treatments by aspect?

Because a major goal of this work is to ensure the practical application of this research to silvicultural prescriptions, there is a

need to bridge the gap between how forest managers and snow hydrologists commonly measure forest structure. We therefore quantify snowpack response to forest structure using two different forest measurement approaches: field-based ground measurements (i.e., basal area) and remotely sensed lidar metrics (described in Section 2).

Basal area is a measurement of the cross-sectional area of tree stems at a standard height of 4.5 feet across a forest stand. Basal area measurements, expressed as square feet per acre, are commonly used by foresters in the USA to estimate tree stand density (Elledge and Barlow, 2018) and to plan forest thinning treatments (Richards, 2014). In contrast, lidar-derived metrics of forest structure tend to focus on canopy structure rather than tree stem density. Therefore, our translation of snow response to different measurements of forest structure aims to support the development of site-specific treatment prescriptions that address snow hydrology in forest management.

2 Materials and methods

2.1 Co-production approach

This project emerged from a collaboration with the Tapash Sustainable Forest Collaborative, one of several forest collaboratives across Washington State. These collaboratives were designed to manage resilient forest ecosystems across ownership boundaries and to build community connections in order to support multiple management goals.

The Tapash Collaborative's geography largely lies within the Yakima River Basin, one of the state's most climate-vulnerable basins due to its heavy reliance on snowpack for water resources and its relatively low elevation headwaters (Donley et al., 2012). Additionally, state and federal management agencies aim to restore forest health and increase wildfire resilience across 1.25 million acres of the Eastern Cascades in the next 20 years through forest treatments such as thinning and prescribed burns (Washington State Department of Natural Resources, 2018a). Much of these forests overlap with critical seasonal snowpacks, which provide 75% of the water supply downstream for endangered fish and a multi-billion-dollar agricultural industry (Li et al., 2017).

We thus worked with the Tapash Forest Collaborative's leadership team to co-develop our research questions and approaches. We began with the premise that prescriptions aimed at increasing wildfire resiliency are currently being implemented at scale across the region and sought to identify which prescriptions enhanced or detracted from hydrologic resiliency.

2.2 Study site

Our study site on Cle Elum Ridge, Washington, USA, is located at the headwaters of the Yakima River Basin on the eastern slopes of the Cascade Mountain Range (Figure 1D). Climate varies strongly within the Yakima Basin; mean annual precipitation (averaged from 1970 to 2000) ranges from 203 to 356 cm along the Cascade Crest headwaters to less than 25 cm at the basin outlet (U.S. Bureau of Reclamation (USBR), 2002; Western Region Climate Center (WRCC), 2007). Most of the annual precipitation falls between October and March, with much of it falling as snow in higher elevation terrain. At lower headwater elevations, such as Cle Elum Ridge, winter temperatures fluctuate around the melting point, thereby shifting precipitation partitioning toward more rain and less snow than at higher-elevation sites (Dickerson-Lange et al., 2023).

Cle Elum Ridge's forested terrain ranges from 840 to 1,000 m in elevation and is dominated by dry grand fir (*Abies grandis*) plant associations, with some Douglas-fir (*Pseudotsuga menziesii*) associations on the driest sites. These forests were managed for industrial timber production until 2014, and extensive coal mining occurred from the late 1800s through the 1950s. Historically, they experienced frequent fire and were dominated by ponderosa pine (*Pinus ponderosa*) and Douglas-fir, with some western larch (*Larix occidentalis*) (Harrod et al., 1999; Wright and Agee, 2004). The ridge is characterized by second- and third-growth forests, a relatively simple structure, and generally denser stands on the north side. Tree heights average ~20 m, with peak heights reaching ~40 m.

Stand structures vary across the ridge, reflecting the changing history of management goals from industrial timber production to coal mining to real estate development and finally to ecological forest management intended to restore forest health, reduce wildfire intensity, and support wildlife, water supplies, and recreational use. The majority of the stands within the study area are low density forests with multiple tree cohorts, typically containing 2–4 large trees per hectare (>50 cm dbh; diameter at breast height). Some single-cohort, young plantations of ponderosa pine and Douglas-fir do exist, but they generally contain older trees. Almost all dry forest stands have experienced multiple partial harvests over the past century, beginning with early selection logging of large ponderosa pines. Since then, most of the stands have been actively managed by previous landowners, either through thinning entries or regeneration harvests. Regeneration harvests have tended to leave significant numbers of retention trees; thus, few pure plantation stands exist on Cle Elum Ridge. Some stands have not been managed in many years and thus have high basal areas and more shade-tolerant species.

2.3 Experimental design and implementation

The spine of Cle Elum Ridge runs west to east, with a higher heat load on the south side than on the relatively steep north side (Dickerson-Lange et al., 2023). We centered the study domain across the spine, enabling comparison of forest density and snowpack interactions as a function of aspect. For each aspect, we worked with a local logging team to thin treatment stands to varying basal area levels (see Section 2.1), creating a gradient of forest densities on both sides of the ridge (Figure 1C). In this study, we quantified forest density as target basal area (referred to as BA in figures; the total area occupied by tree stems within a stand, in $ft^2\ acre^{-1}$), rather than a metric such as canopy cover, because basal area is directly used to develop forest prescriptions. We collected snow-on lidar data before and after the thinning treatments were completed (Figures 1A,B).

We evaluated the effects of forest density and aspect on snowpack response by measuring snow storage magnitude and duration before and after experimental forest treatments. We directly tested the forest management hypothesis that lower forest density on north facing slopes would increase snowpack retention in this region, as suggested by Dickerson-Lange et al. (2023) based on observed differences in snow storage between gaps and adjacent forests.

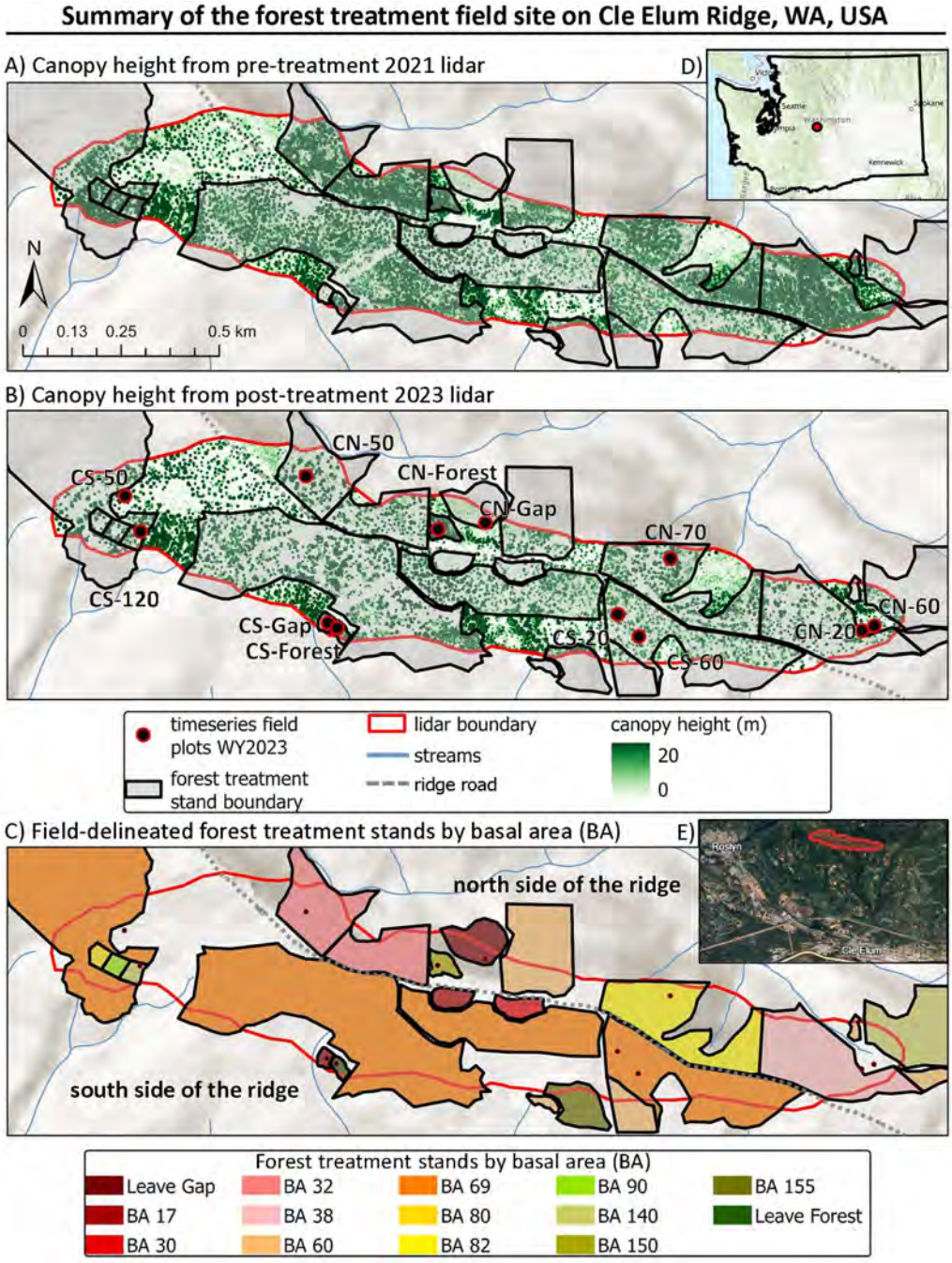

FIGURE 1
Summary of the forest treatment field study domain on Cle Elum Ridge, WA, USA, showing lidar-derived canopy height: **(A)** before and **(B)** after forest treatments, and **(C)** field-delineated treatment stands color-coded by basal area (BA; ft^2 $acre^{-1}$). The lidar boundary is shown in red, forest treatment boundaries are outlined in black, snow depth timeseries field plots from WY2023 appear as red-outlined black circles, and the ridge road is shown as a gray dashed line. Different basal area levels of the forest treatment are depicted with color coding. Cle Elum Ridge is located **(D)** on the eastern side of the Cascades in Washington State and **(E)** directly north of Cle Elum, imagery © 2023 Google Earth.

Forest thinning treatments were implemented on Cle Elum Ridge during water year 2022 (WY; 1 October 2021 to 30 September 2022). The treatment area comprises smaller field-delineated treatment stands, each with a different stand prescription and area (Table 1). Prescriptions included a gradient of thinning intensity, ranging from dense (i.e., no thinning) to open stands based on basal area on the north and south sides of Cle Elum Ridge. Trees were individually marked for retention in the field using a Spiegel Relaskop with a 20 basal area factor, targeting basal areas between 20 and 155 ft^2 $acre^{-1}$, depending on the treatment unit (Table 1). Forest prescriptions followed a forest management approach centered on variably retaining individuals, clumps, and openings (referred to collectively as ICO; Churchill et al., 2016) to recover a heterogeneous mosaic of forest structure reflective of historical

TABLE 1 A summary of the forest treatments on Cle Elum Ridge by aspect and the corresponding timeseries identification code (ID) for field plots inside each field-delineated treatment stand.

Field-delineated forest treatment stand basal area (BA) $ft^2\ acre^{-1}$	Type of forest treatments performed in each stand	Date of treatment	Snow depth timeseries ID* from field plots within the treatment stand	Total areas (rounded to 0.1 acres and 10 m^2)	
				acres	m^2
Total area				147	594,940
Total area not in the treatment stands				40	161,730
Total area of the treatment stands combined				107	433,200
The south side of the ridge				90.3	365,430
The total area not in the treatment stands on the south side				23.8	96,400
Total area of the treatment stands combined on the south side				66.5	269,030
Leave gap	None	–	CS-Gap**	0.3	1,040
Leave forest (*with a BA of 155*)	None	–	CS-Forest**	0.2	880
BA 17	Thinning; Mastication	June 2022	–	0.9	3,590
BA 30	None	–	–	1.1	4,480
BA 60	Thinning	June 2022	–	0.4	1,780
BA 69	Thinning; Mastication	Thinning: July–December 2021, July 2022, March 2023; Mastication: June 2022	CS-20*, CS-50*, CS-60*	53.6	216,960
BA 80	Thinning	November 2021		0.5	1,920
BA 90	Thinning; Mastication	November 2021	–	0.5	1,900
BA 140	Thinning	November 2021	CS-120*	0.5	1,820
BA 155	None	–	–	0.3	1,210
The north side of the ridge				56.7	229,510
The total area not in the treatment stands on the north side				16.1	65,330
Total area of the treatment stands combined on the north side				40.6	164,180
Leave gap	None	–	CN-Gap**	1.2	4,870
Leave forest (*with a BA of 150*)	None	–	CN-Forest**	0.7	2,860
BA 32	Thinning	June 2022	CN-50*	10.1	40,990
BA 38	Thinning	December 2022	CN-20*	9.6	38,790
BA 60	Thinning	August 2022	–	2.9	11,620
BA 82	Thinning	September 2022	CN-70*	10.4	41,910
BA 140	Thinning	November 2021	CN-60*	1.0	3,950

*The timeseries IDs combine the site (C for Cle Elum Ridge) and aspect (N or S) with a number that represents the basal area determined in the field at the plot scale. These values vary from the basal area values of the forest treatment stands in which they are located due to the difference in forest characteristics averaged at the spatial scale of a plot (10 × 10 m; ~0.02 acres) versus a treatment stand (typically ~0.2–10 acres with one larger stand of 53 acres). **Same plots with snow observations from WY2020 and WY2021, reported in Dickerson-Lange et al. (2023).

reference conditions, rather than evenly spaced trees (Churchill et al., 2013). Additionally, larger individual trees and more fire-resilient tree species, such as ponderosa pine, were retained. Smaller trees, known as ladder fuels, and less fire-resistant species, such as Douglas-fir and grand fir, were selectively thinned or targeted for removal.

As this experiment occurred within the context of an active, multi-objective community forest project, on the ground decisions during the treatment and post-treatment stages shifted the original basal area targets while retaining a gradient of thinning levels across slope aspects. Post-treatment basal areas for treatment stands represent the average basal area per stand and were calculated using a combination of ground measurements and Plot Hound software (SilviaTerra, 2017). Stand basal area metrics on the north and south sides of Cle Elum Ridge are presented in Table 1. In some stands, brush, small trees, and logging slash were masticated to reduce the size of ground-level fuels, which can otherwise increase wildfire severity and spread. Due to steep slopes, mastication was not achievable in all

experimental stands. As such, the forest treatments we present here reflect practicable forestry prescriptions for fire-resilient, dry forests in the Eastern Cascades.

2.3.1 Snow depth timeseries field plots

We monitored snow depth at 12 timeseries field plots on Cle Elum Ridge, with six plots on each side of the ridge (Figures 1B,C). Four legacy plots were established by Dickerson-Lange et al. (2023) in WY2020 and WY2021 and retained for this study in WY2023. Plot IDs combine Cle Elum Ridge (C), aspect (N for north, S for south), and either a descriptor ("Forest" or "Gap") or a number (basal area target; $ft^2\ acre^{-1}$). The legacy plots represent untreated conditions, with paired "Forest" and "Gap" sites on both the north and south aspects (CN-Forest, CN-Gap, CS-Forest, CS-Gap). Thinning treatments did not alter their forest structure. In WY2023, we added eight new plots to capture snow responses across a gradient of forest thinning treatments (Table 1). These plots were located in treatment units prescribed for specific stand-level basal area targets. North side plots were placed in units prescribed for 20, 50, 60, and 70 $ft^2\ acre^{-1}$ (CN-20, CN-50, CN-60, CN-70), while south side plots were placed in units prescribed for 20, 50, 60, and 120 $ft^2\ acre^{-1}$ (CS-20, CS-50, CS-60, CS-120). Because each timeseries plot samples only a small footprint (10 m x 10 m; ~0.02 acres) within a much larger treatment unit (typically 0.2 to 10 acres), measured basal area at the plot may differ from the prescribed stand-level target (see Table 1 footnote).

In each field plot, we collected daily observations of snow depth, snow presence, and air temperature. We deployed three snow measurement poles within each plot within the view of time-lapse cameras. The three poles were strategically placed across the plots to cover the largest variability in forest cover. One pole was placed against the base of a tree in the plot, a second below the edge of the tree canopy, and a third in the center of the most open area of the plot. We created a daily timeseries of snow depth from visual inspection of the time-lapse images for each pole, rounded to the nearest 5 cm. We took hemispherical photos at each snow depth pole, which we used to calculate the sky view fraction directly above each pole (see Dickerson-Lange et al., 2023 for methods).

2.4 Lidar data

We used three lidar datasets to quantify forest structure and snow depth before and after forest treatments on Cle Elum Ridge, Washington. We obtained snow-off terrain data from the Washington Department of Natural Resources (WA DNR) lidar portal, combining two publicly available datasets to cover the entire study domain: *Yakima Basin North 2018* (Washington Geological Survey, 2018) and *Teanaway 2015* (Washington Geological Survey, 2015). These datasets were collected and processed by WA DNR contractors and have a point density of >8 points m^{-2} (Gleason, 2018; Norton, 2015).

The pre-treatment snow-on lidar was collected on 1 April 2021 by the National Center for Airborne Laser Mapping (NCALM) using airborne lidar (dataset named *SOUT_GEG/F*; Lumbrazo, 2021). The post-treatment snow-on lidar was collected on 6 March 2023 by the NHERI Natural Hazards Reconnaissance (RAPID) facility (Berman et al., 2020; Wartman et al., 2020) using a drone-based system (Freefly Alta X equipped with the Phoenix MiniRanger; Lumbrazo et al., 2025). Both snow-on surveys were conducted as close to peak SWE as possible to capture maximum seasonal snow accumulation. Each lidar dataset was independently acquired and processed by the corresponding agency, with mean point densities of 11.9 points m^{-2} for the 2021 NCALM dataset and 100 points m^{-2} for the 2023 RAPID dataset (Lumbrazo, 2021; Lumbrazo et al., 2025). Hereafter, we refer to these as the pre-treatment and post-treatment lidar datasets.

We used the 1 m-resolution gridded digital terrain models and digital surface models from each dataset for analysis, excluding roads and applying a 5 m buffer on either side to avoid artifacts from plowing. From these gridded surfaces, we (1) derived landscape metrics from the snow-off lidar, (2) quantified changes in forest structure from the pre- and post-treatment lidar, (3) calculated snow depth differences independent of forest structure using the pre- and post-treatment lidar, and (4) estimated the associated water storage benefit from forest thinning using the post-treatment lidar.

2.4.1 Lidar-defined landscape metrics

We used snow-off lidar data to calculate landscape metrics, including elevation, slope angle, and slope aspect (Figure 2). From previous research in this region (Dickerson-Lange et al., 2023), we know that the radiative heat a specific location receives affects snow ablation rates and is particularly important in influencing snow depth at this elevation (Figure 2A). Thus, we carefully defined the slope aspect (hereafter, aspect) of Cle Elum Ridge in two main ways. First, we used the spine of Cle Elum Ridge, which runs west-east, to define the north and south sides of the ridge (Figure 2F). This simple approach is the primary method used by foresters in the field to define aspects at this site.

We also defined aspect at a smaller spatial scale (1 m) by calculating the Diurnal Anisotropic Heating Index (DAH), referred to as heat index, which captures variability in heat inputs due to both slope angle (Figure 2B) and aspect (Figure 2C) (Cristea et al., 2017). Therefore, we calculated DAH as follows:

$$DAH = \cos\left(\alpha_{\max} - \alpha\right) * \arctan\left(\beta\right), \begin{matrix} where\ DAH < 0,\ low\ heat\ index \\ where\ DAH \geq 0, high\ heat\ index \end{matrix} \quad (1)$$

Where $\alpha_{\max}$ = 202.5° (SSW) is the aspect that receives the most heat, and α is the aspect at the location, and β is the slope angle in radians. DAH ranges from −1 to 1 and is zero in flat terrain (Figure 2D). The highest DAH values are on steep southwest-facing slopes, and the lowest are on steep northeast-facing slopes (Cristea et al., 2017). We classified the heat index into high and low categories: areas with DAH ≥ 0 indicate a high heat index, and those with DAH < 0 indicate a low heat index (Eq. 1; Figure 2E).

When we compared the resulting binary heat index map (Figure 2E) with the field-based classification of aspect, which uses the ridge's spine to define the sides of Cle Elum Ridge (Figure 2F), we found strong agreement, particularly on the north side of the ridge. Although some areas on the south side of the ridge show low heat index values due to local topographic shading (Figure 2E), we found that these differences had a negligible impact on the analysis. Therefore, we proceed to use the ridge's spine to define the sides of the

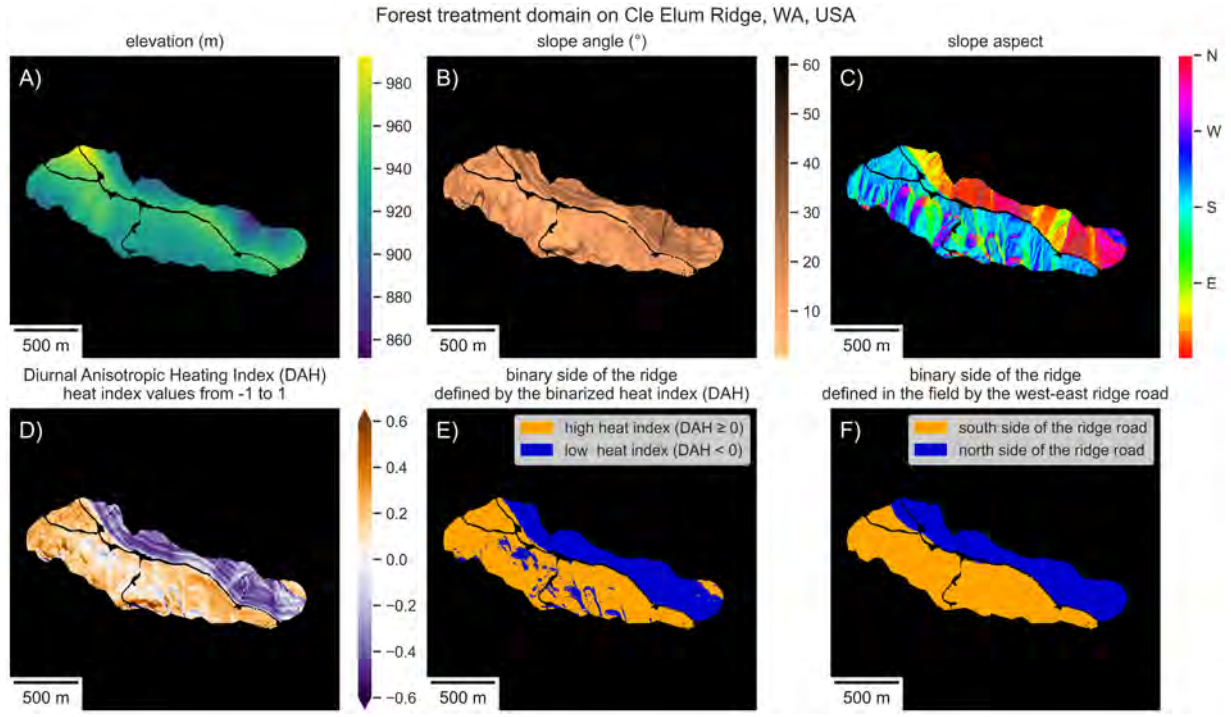

FIGURE 2
The **(A)** elevation (m), **(B)** slope angle (degrees), and **(C)** slope aspect (N/W/S/E) across Cle Elum Ridge. The dominant aspects of Cle Elum Ridge are defined in two main ways. First, the **(D)** landscape Diurnal Anisotropic Heating Index (DAH) is calculated for the entire domain, and **(E)** then binarized into two primary categories: low heat index terrain (DAH < 0; blue) and high heat index terrain (DAH ≥ 0; orange). Second, the main west–east ridge that defines the Cle Elum Ridge domain is used to divide the terrain **(F)** into the north side of the ridge (blue) and the south side (orange).

ridge for this analysis, as the foresters do in the field at this site (Figure 2F).

2.4.2 Lidar-defined change in forest structure

To determine canopy height from the pre- and post-treatment lidar datasets, we computed the difference between the snow-off digital terrain model and the snow-on digital surface models (Figures 3A,B). Additionally, we differenced the two canopy height maps from before and after the forest treatments to produce a canopy height difference map (Figure 3C). From this map, we can identify where forest structure changed, assuming that positive values in the difference map reflect snow depth and vegetation growth, while negative values greater than 3 m indicate forest cover change (Figure 3C). Because snow depth on Cle Elum Ridge was rarely greater than 2 m during either lidar acquisition, we thresholded canopy calculations to heights ≥ 3 m.

We calculated the percentage of canopy cover within each treatment stand both before and after the forest treatments (Figures 3G,H). We defined canopy cover as all pixels taller than 3 m and computed the proportion of these pixels within each stand on the south (Figure 3G) and north (Figure 3H) sides of Cle Elum Ridge. Then, we compared pre-treatment canopy cover to post-treatment values for each stand.

As another method to quantify changes in forest structure, we calculated the distance to canopy edge (DCE). We followed methods similar to those described by Mazzotti et al. (2019), in which each grid cell is assigned a distance to a canopy element (Figures 3D,E). A canopy element is defined as any grid cell that contains a canopy pixel above 3 m in height. The resulting DCE is the distance, in meters, from the canopy edge, where the edge is defined as zero. Grid cells in the open are increasingly positive the further they are from the canopy edge, and those under the canopy are increasingly negative. The larger the positive number, the greater the gap; the larger the negative number, the denser the surrounding forest. We computed continuous rasters of the pre-treatment (Figure 3D) and post-treatment (Figure 3E) canopy structure. For some analyses, we grouped DCE values into five classifications: dense forest (DCE ≤ -8 m), sparse forest (-8 m < DCE ≤ -2 m), forest edge (-2 m < DCE ≤ 2 m), small gap (2 m < DCE ≤ 8 m), and large gap (DCE > 8 m). Small gaps roughly correspond to diameters of 4 to 16 m, and large gaps to diameters >16 m, assuming circular gaps with the pixel near the gap center. Although irregularly shaped gaps may have different dimensions for the same DCE value, we based our diameter estimates on this circular-gap assumption, since gap diameter is a standard way to describe canopy openings.

To evaluate how much the forest structure changed as a result of the forest treatments, we differenced the pre- and post-treatment DCE maps to produce a difference in DCE map (ΔDCE) (Figure 3F). We reclassified ΔDCE into six categories to capture qualitative changes in forest structure before and after the forest treatments (Table 2). This step accounted for the fact that the same ΔDCE value can result from different forest changes.

When a pixel started with a negative pre-treatment DCE value and became a more negative value post-treatment, it indicated forest growth, with the forest edge moving further away (ΔDCE category: *forest-to-denser-forest*; Table 2). If the negative pre-treatment DCE

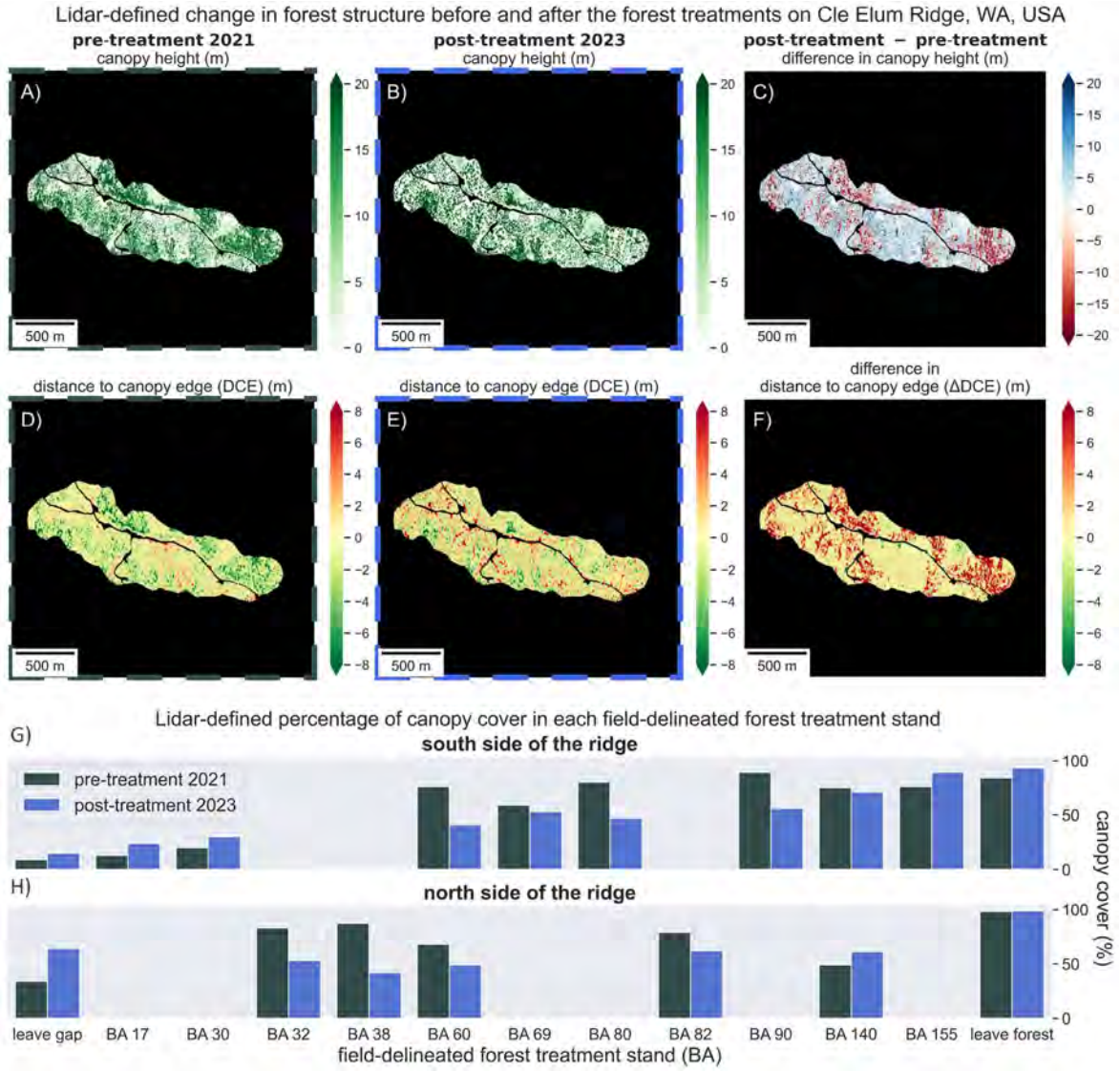

FIGURE 3
Lidar-based change in forest structure between pre-treatment 2021 and post-treatment 2023 lidar, including **(A)** pre-treatment canopy height (m) in 2021, **(B)** post-treatment canopy height (m) in 2023, **(C)** difference in canopy height (m) calculated as post-treatment 2023 minus pre-treatment 2021, **(D)** the pre-treatment distance to canopy edge (DCE; m), **(E)** the post-treatment DCE (m), **(F)** the difference in DCE (ΔDCE; m), and the lidar-derived percentage of canopy cover (%) pre-treatment 2021 (slate gray) and post-treatment 2023 (blue), within the field-delineated forest treatment stands (BA) on the **(G)** south and **(H)** north sides of Cle Elum Ridge.

became a smaller negative post-treatment value, the forest thinned, and the edge moved closer (ΔDCE category: *forest-to-forest-edge*; Table 2). Pixels with little to no change in DCE were classified as the ΔDCE category: *no-forest-change* (Table 2). For positive pre-treatment DCE values, a decrease post-treatment indicated that the forest edge moved closer, making the area less open (ΔDCE category: *open-to-less-open*; Table 2), while an increase indicated a more open canopy (ΔDCE category: *open-to-more-open*; Table 2). If a negative pre-treatment DCE became positive post-treatment, the pixel shifted from forest to open (ΔDCE category: *forest-to-open*; Table 2).

We used these ΔDCE categories to create lidar-defined treated areas on Cle Elum Ridge (Figure 4). We defined the untreated areas using ΔDCE categories that identified *no-forest-change* and forest growth, such as *forest-to-denser-forest* and *open-to-less-open*. We defined the treated areas based on ΔDCE categories that identified forest thinning, such as *open-to-more-open*, *forest-to-forest-edge*, and *forest-to-open* (Figure 4). In subsequent calculations, we used the ΔDCE categories to define treated and untreated areas since they reflect the actual locations on the ground where forest structure changed as a result of the treatments (Figure 4B), in contrast to the field-delineated treatment stands, which are field-based estimates of the treatment domains (Figure 1C).

2.4.3 Lidar-defined change in snow depth

To determine snow depth from the pre- and post-treatment lidar datasets, we differenced the snow-off digital terrain model from the snow-on digital terrain models, assuming the ground surface did not change between the two lidar flights. We used the snow depth values

TABLE 2 The ΔDCE categories are used to classify six types of changes in forest structure following forest treatments.

ΔDCE category	Description of forest change	Forest growth or thinning	Pre-treatment 2021 DCE (m)	Post-treatment 2023 DCE (m)	ΔDCE value
Forest-to-denser-forest	Started as forest and the forest edge became further away due to growth at edge	Growth	<0	<<0	–
Forest-to-forest-edge	Started as forest and the forest edge got closer due to thinning	Thinning	<<0	<0	+
No-forest-change	No change in classification				Near 0
Open-to-less-open	Started in open and became less open (closer to the edge)	Growth	>>0	>0	–
Open-to-more-open	Started in open and became more open (further from edge)	Thinning	>0	>>0	+
Forest-to-open	Started in forest and became open	Thinning	<0	>0	+

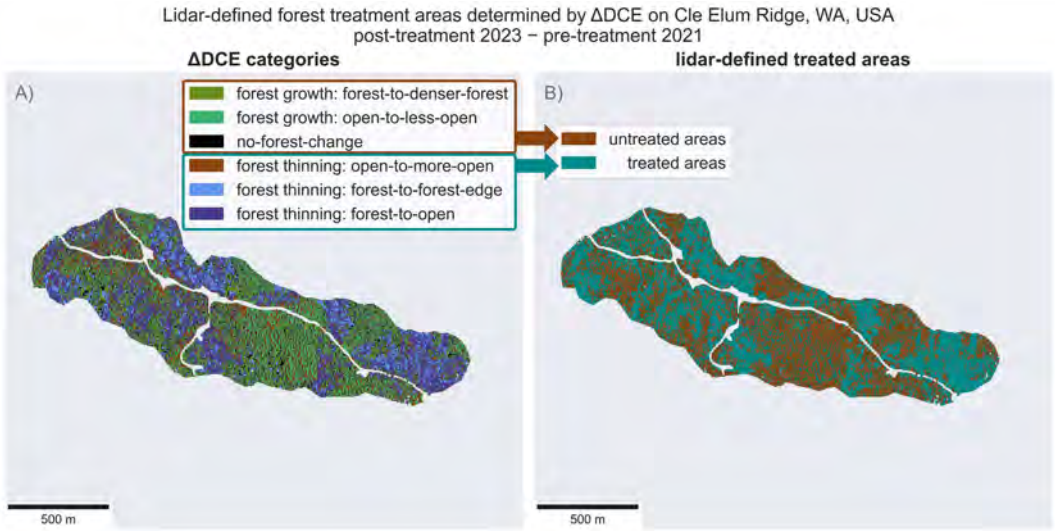

FIGURE 4
The change in forest structure resulting from the forest treatments was quantified using the **(A)** difference in distance to canopy edge (ΔDCE) categories, which we used to determine the **(B)** untreated (brown) and treated (cyan) areas on Cle Elum Ridge. ΔDCE categories indicating forest growth or no change define the untreated areas, while categories indicating forest thinning define the treated areas.

for both years from the ΔDCE category *no-forest-change* to compute mean values of 0.17 and 0.20 m and standard deviations of 0.23 and 0.24 for pre-treatment 2021 and post-treatment 2023, respectively. We used these values to normalize snow depth for all pixels in each year as described below.

Snow depth maps from two different years must be compared carefully, as meteorological conditions, such as changes in air temperature and precipitation, can cause natural variations in snow depth from year to year at a single location. These variations make it challenging to compare snow depth directly and to isolate the effects of forest treatments from natural variations in snow depth. Previous studies have shown that while snow depth totals might change, snow depth patterns persist (Pflug and Lundquist, 2020; Sturm and Wagner, 2010). Thus, we normalized by the mean snow depth in unchanged areas across the study domain to compare snow depth maps and isolate the influence of changes in snow depth patterns resulting from changes in forest structure. We calculated the Standardized Depth Value (SDV) from Sturm and Wagner (2010), which defines SDV_i at any grid cell, i, as:

$$SDV_i = \frac{(d_i - \mu_d)}{\sigma_d} \quad (2)$$

Where d_i is the observed snow depth at any grid cell, μ_d is the domain mean snow depth, and σ_d is the domain snow depth standard deviation (Pflug and Lundquist, 2020; Sturm and Wagner, 2010). Typically, the domain for computing mean and standard

deviation is defined as the entire lidar domain, assuming that landscape-scale metrics that influence snow depth—such as complex topography, aspect, and canopy cover—are unchanged between lidar flights. In our situation, the dominant control on snow depth is forest structure, which changes due to forest treatments. Thus, we defined our domain for computing mean and standard deviations as the lidar domain which remained unchanged from the forest treatments, previously defined as the ΔDCE category *no-forest-change*, (Table 2; Figure 4A). We used the mean and standard deviation of the *no-forest-change* ΔDCE category to calculate the pre- and post-treatment SDVs. We subtracted the post-treatment SDV from the pre-treatment SDV to assess changes in normalized snow depth before and after treatment.

2.4.4 Lidar ground validation and snow density measurements for SWE calculations

We collected ground-based measurements of snow depth to validate the post-treatment 2023 snow-on lidar and snow density to calculate SWE for estimating total water storage. Ground validation included snow pit observations that characterized snow density and stratigraphy across both aspects and various forest structures (Table 3).

We excavated four snow pits, two per aspect, during the post-treatment lidar flight. At each pit, we sampled every 10 cm using a 250-cc cutter to determine snow density, which we aggregated to calculate the average bulk snow density per pit (Table 3). We report snow density as the percentage of the snowpack composed of liquid water. The average density across all pits was 31% (i.e., 310 kg m^{-3}), with higher values on south-facing slopes (34%) than north-facing slopes (29%), consistent with greater solar exposure and melt-refreeze cycles on the south aspect (Table 3). The snowpack generally consisted of two layers: a lower layer of rounded grains and an upper layer of fresh, lower-density snow.

We used these observations of snow density to estimate SWE by multiplying the lidar-derived snow depths by the corresponding bulk density from the snow pit measurements (i.e., SWE = snow depth × snow density). These SWE values represent the total amount of water stored in the snowpack and form the basis for evaluating how snow storage differed by aspect before and after forest treatments.

TABLE 3 Post-treatment 6 March 2023 lidar flight snow pits.

Snow pit location	Snow depth	Snow density (%)		Snow pit notes
		Range	Average	
South side of the ridge	32 cm	25–39%	33%	Pit in the open with an ice layer
South side of the ridge	65 cm	19–44%	35%	Pit between 2 small ponderosa pines
North side of the ridge	71 cm	14–38%	29%	Pit in the open with no ice layers
North side of the ridge	54 cm	18–36%	29%	Pit in the open with no ice layers

3 Results

3.1 What is the snow depth response to a gradient of forest thinning treatments as a function of aspect?

3.1.1 Plot scale: defined by the field-measured basal area

To understand the snow depth response to the gradient of forest thinning treatments at the plot scale, we visualize snow depth from the timeseries field plots on Cle Elum Ridge during WY2023 (Figure 5). We visualize the three snow depth poles within each field plot first as a function of their local basal area, where the plot names indicate the basal area and side of the ridge, such as CS-20 for a basal area of 20 on the south side and CN-50 for a basal area of 50 on the north side (Figures 5A, B), and second as a function of the sky view fraction calculated by hemispherical photography at each individual pole (Figures 5C,D).

When we visualize the three snow depth poles within each field plot as a function of their basal area, no clear relationship emerges between snow depth and the basal area of forest thinning on either side of the ridge (Figures 5A,B). On the south side of the ridge, two of the snow depth poles in the CS-20 plot have a deeper snowpack throughout the season (addressed further in the Discussion Section 4.3), while the remaining snow depth poles on the south side cluster together, with a relatively shallow snowpack below 50 cm that frequently melts out during the snow season (Figure 5A). On the north side of the ridge, the snow depth poles with the highest basal areas show some grouping with the lowest snow depth throughout the season (Figure 5B). However, across the entire north side of the ridge, snow depths and durations vary among poles in the CN-20, CN-50, and CN-60 plots, making it difficult to identify a clear relationship between snow depth and the level of forest thinning within this basal area range (Figure 5B).

In contrast, when we visualize the three snow depth poles in each timeseries plot as a function of the sky view fraction, we observe that snow depth roughly increases with increasing sky view fraction (Figures 5C,D). Specifically, on the north side of the ridge, there is a clear relationship between snow depth and sky view fraction, with a higher sky view fraction above a snow depth pole correlating with deeper snow depth at that location throughout the snow season (Figure 5D).

3.1.2 Stand scale: defined by the field-delineated forest treatment stands and the lidar-defined forest treated areas

To understand the snow depth response to the gradient of forest thinning treatments at the stand scale, we visualize snow depth and forest structure metrics from the post-treatment 2023 lidar data for the forest treatment stands on Cle Elum Ridge (Figure 6). The forest treatment stands cover a range of basal areas from 17 to 155, which we visualize as Cumulative Distribution Functions (CDFs) of snow depth (Figures 6A,B) and DCE (Figures 6C,D) for each forest treatment stand.

While the forest treatment stands represent a range of thinning, with basal area values from 17 to 155, this thinning gradient is not

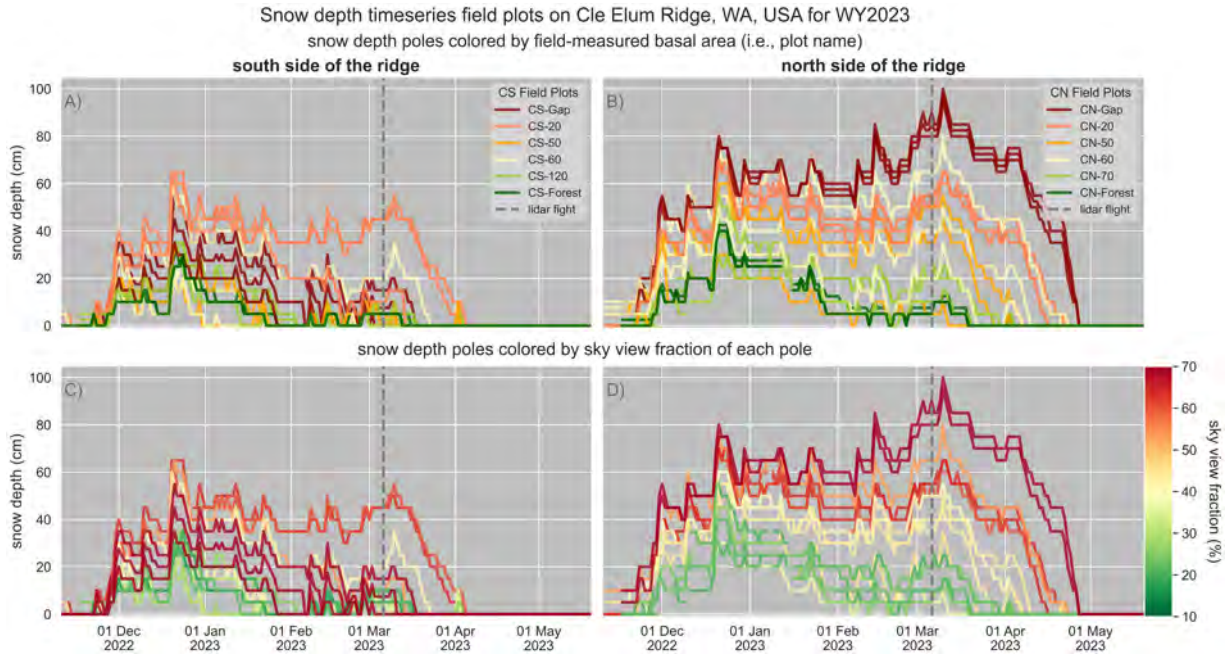

FIGURE 5
Post-treatment snow depth timeseries from field plots on Cle Elum Ridge during WY2023. Panels **(A, B)** show snow depth (cm) grouped by plot-scale basal area, and panels **(C, D)** show snow depth (cm) grouped by sky view fraction (%) derived from hemispherical photography for each snow depth pole. Panels **(A, C)** correspond to the south side of the ridge, and panels **(B, D)** correspond to the north side. Each line represents an individual snow depth pole.

reflected in the distribution of DCE within each treatment unit (Figures 6C,D). Instead, the majority of forest treatment stands consist of a mix of gaps and non-gaps, leading to similar DCE distributions (Figures 6C,D) and, consequently, a similar snow depth response (Figures 6A,B). This pattern is further evident when examining the percentage of canopy cover in each treatment unit; the majority of the stands have similar canopy cover, ranging from 40 to 60% (Figures 6E,F). However, treatment stands at the extremes of thinning practices, such as the Leave forest stand (with a BA of 150) and the BA 155 stand, have a closed canopy with over 90% canopy cover (Figures 6E,F). These stands also have the least amount of snow, by far, on both sides of the ridge (Figures 6A,B).

Since the forest treatment stands do not show much separation in terms of DCE distributions, and the snow response to the gradient of thinning, as defined by basal area, is nonlinear (Figure 6), we visualize the change in forest structure resulting from the forest treatments as the ΔDCE before and after the forest treatments in the six categories described in Table 2 and Figure 4.

When we visualize snow depth responses to changes in forest structure as ΔDCE categories (Figure 4A), we observe greater snow depth after the forest treatments in areas where the canopy was opened on both sides of the ridge (Figure 7). These categories include forested areas that became less dense or shifted closer to the forest edge (*forest-to-forest-edge* in light blue), open areas that became more open (*open-to-more-open* in brown), and forested locations that transitioned to fully open (*forest-to-open* in dark blue) (Figure 7). In contrast, there was little to no change in normalized snow depth in areas where the forest structure did not change (*no-forest-change* in black). There was slightly less snow after the forest treatments, where the forest became more forested (*forest-to-denser-forest* in olive green) and where the open areas became less open (*open-to-less-open* in light green) (Figure 7). Although similar patterns occurred on both sides of Cle Elum Ridge, the snow depth response to ΔDCE was more distinct and greater on the north side (Figure 7B).

3.2 What is the snow depth response to the overall forest structure across the site by aspect?

Since the snow depth response is more strongly linked to changes in local forest structure (Figure 7) than to area-averaged basal area within individual treatment areas (Figure 6), we leverage lidar data to assess the snow depth response to the resulting forest structure. To understand the overall snow depth response to forest structure on Cle Elum Ridge, regardless of the mapped forest treatment stands, we visualize CDFs of snow depth in groups of the DCE over the entire ridge before (Figures 8A–C) and after (Figures 8D–F) the forest treatments. The effect of the forest treatments on the overall forest structure is indicated by the total number of grid cells classified for each DCE group (shown as *n* in the legend of Figures 8A,C,D,F) in 2021 and 2023.

On both sides of the ridge before and after the forest treatments, the deepest snowpack occurs in small gaps between 4 and 16 m in diameter (i.e., 2 m < DCE ≤ 8 m), and the shallowest snowpack occurs in dense and sparse forested areas (Figures 8A,C,D,F). On the north side of the ridge, before and after the forest treatments, and on the south side after the forest treatments, we find that the snowpack within 2 m of forest edges is deeper than in forested areas and shallower than in small gaps. We generally observe deeper snowpack

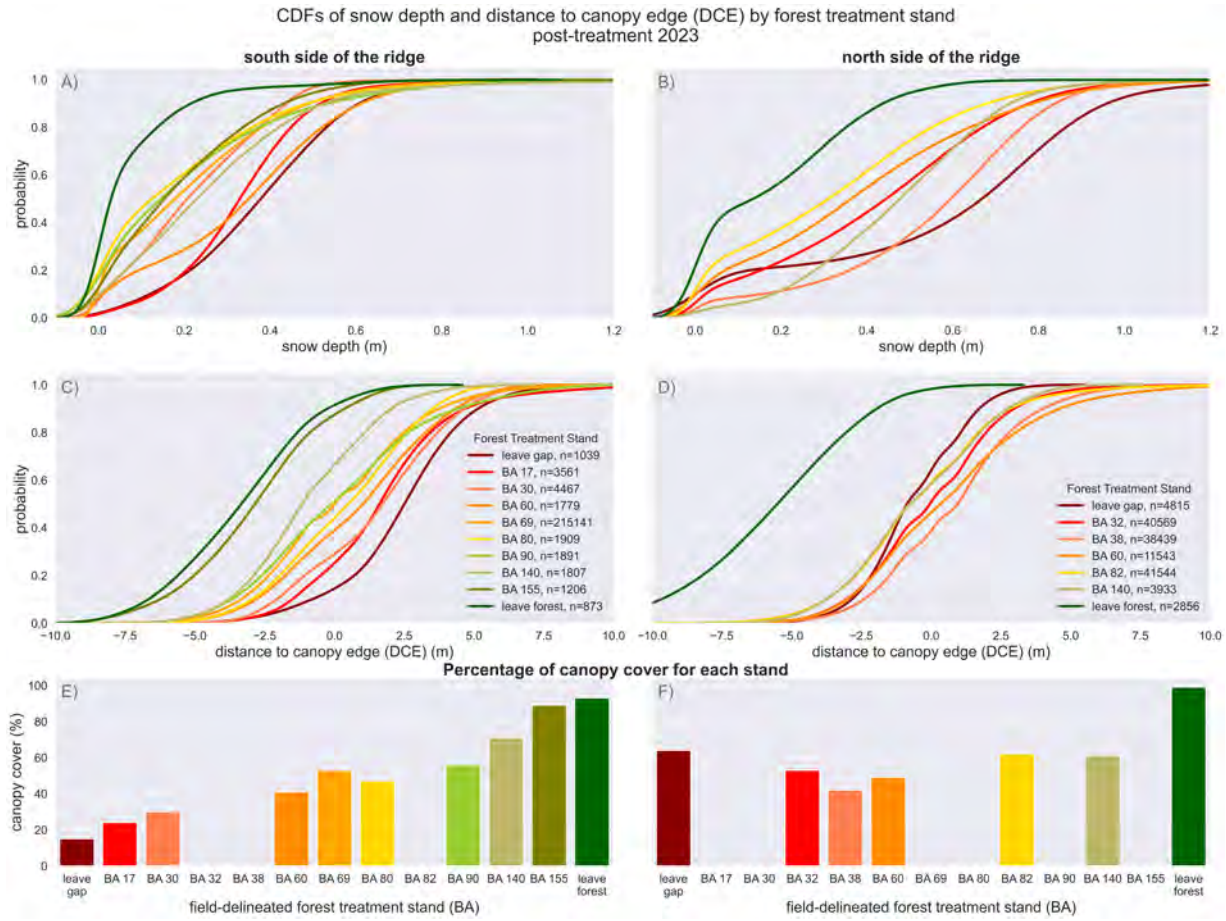

FIGURE 6
CDFs of the forest treatment stands on the south and north sides of Cle Elum Ridge. Panels **(A, B)** show CDFs of snow depth (m), panels **(C, D)** show CDFs of distance to canopy edge (DCE; m), and panels **(E, F)** show lidar-derived canopy cover (%). Panels **(A, C, E)** correspond to the south side of the ridge, and panels **(B, D, F)** correspond to the north side. Lines are color-matched to the basal area (BA) of each field-delineated forest treatment stand.

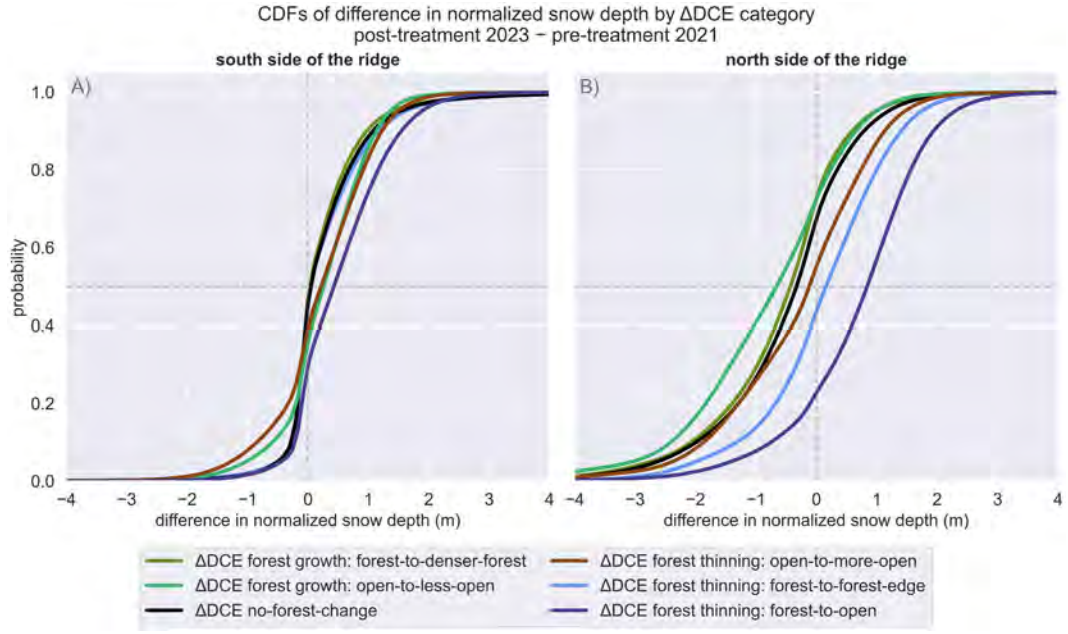

FIGURE 7
CDFs of the difference in normalized snow depth (i.e., the number of standard deviations away from the mean; m) for each ΔDCE category before and after the forest treatments on the **(A)** south and **(B)** north sides of Cle Elum Ridge. See Figure 4A for a map and Table 2 for a description of the ΔDCE categories.

in large gaps (>16 m diameter; DCE > 8 m) compared to forested areas, with the exception of the north side of the ridge before treatment (Figure 8C), but note that the sample size for large gaps on the north side of the ridge before the forest treatments is very small (Figures 8B,C; n = 80 grid cells). Given that the sample sizes for large gaps are relatively small within the analysis domain, these results do not provide evidence for snow depth response in large clearings. Furthermore, we caution against interpreting snow depth results in the large gaps, which are included in the analysis because they are primarily adjacent to the main forest road, particularly on the north side (Figure 8E), where solar exposure is not representative of conditions further downslope.

3.3 How does total snow storage change before and after the forest treatments by aspect?

3.3.1 Comparing Standardized Depth Values (SDV) post-treatment 2023 and pre-treatment 2021

We compare total snow storage on Cle Elum Ridge before and after the forest treatments using the SDV and find median SDV differences of 0.37 on the south side and 0.22 on the north side (Figure 9A). Notably, SDV represents the number of standard deviations away from the mean rather than the physical snow depth (Eq. 2). As described in Section 2.4.3, this normalization enables direct comparison between north and south aspects by accounting for natural differences in overall snow accumulation. The overall positive SDV difference values confirm that, across Cle Elum Ridge, snow depth is generally deeper after the forest treatments (Figure 9A).

When we compare total snow storage between untreated and treated areas (Figure 4B), we find median SDV differences of 0.10 in untreated areas and 0.53 in treated areas (Figure 9B). These results indicate that there is nearly no change in snow depth between the two years in untreated areas, whereas treated areas show a deeper snowpack in 2023 following forest treatments.

When we isolate the untreated and treated areas on the south side of the ridge, we find median SDV differences of 0.31 in the untreated areas and 0.45 in the treated areas, indicating deeper snow in both areas after the 2023 forest treatments (Figure 9C). When we isolate the untreated and treated areas on the north side of the ridge, we find a median SDV difference of –0.40 in the untreated areas and 0.62 in the treated areas (Figure 9D). These numbers indicate that there was less snow in the untreated areas and more snow in the treated areas after the treatments compared to before the treatments on the north side of the ridge.

3.3.2 Calculating total water storage (acre-feet) post-treatment 2023

Using the lidar-derived forest treated areas defined by ΔDCE categories on each side of the ridge (Figure 4B), we calculate SWE difference per unit area during 2023 (post-treatment) to infer water storage gains linked to forest treatments (Table 4). Assuming a uniform snow density of 31% across Cle Elum Ridge (Table 3), we find an increase in water storage following treatment on both aspects: 15 mm (+16%) of SWE per m^2 more on the south side and 37 mm (+30%) more on the north side (Table 4). These SWE per unit area values are normalized to spatial extent rather than to year to year climate variability and represent differences observed in 2023 only. This normalization allows direct comparisons between groups and a clearer assessment of treatment effects by aspect. We estimate total water storage in treated and untreated areas by multiplying SWE per unit area by

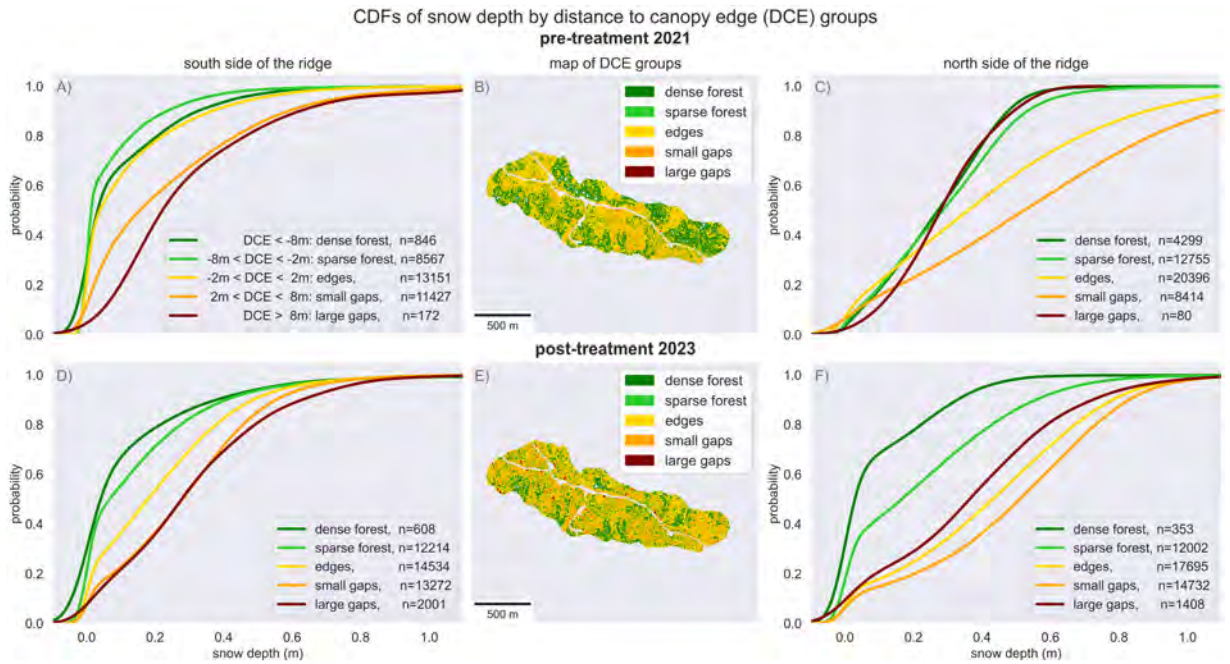

FIGURE 8
CDFs of lidar-derived snow depth (m) for pre-treatment 2021 and post-treatment 2023 lidar on Cle Elum Ridge. Panels **(A,D)** show CDFs for the south side of the ridge and panels **(C,F)** for the north side, with each line representing a distance to canopy edge (DCE; m) group (n indicates the number of grid cells per group). Corresponding maps of DCE groups for each year are shown in panels **(B)** and **(E)**.

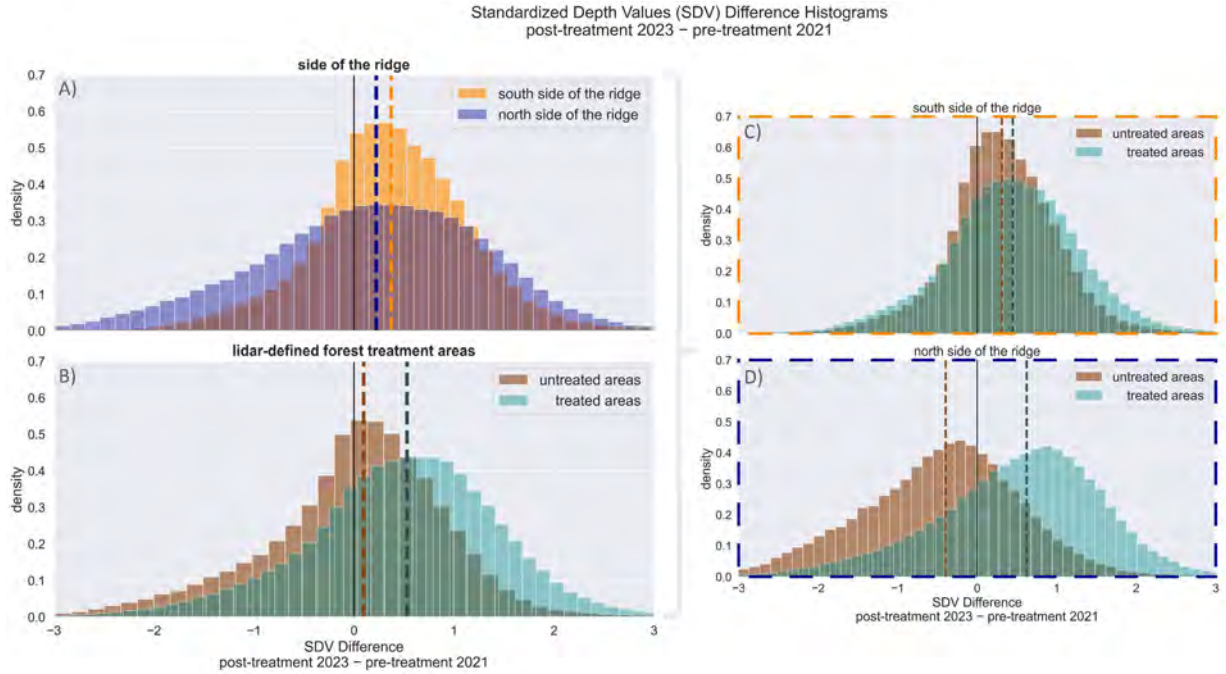

FIGURE 9
Histograms of the difference in Standardized Depth Values (SDV) between post-treatment 2023 and pre-treatment 2021, separated by: **(A)** the south and north sides of the ridge for the entire domain, **(B)** untreated and treated areas for the entire domain, **(C)** untreated and treated areas on the south side of the ridge, and **(D)** untreated and treated areas on the north side of the ridge. The median of each histogram is shown as a dashed vertical line in the color corresponding to that domain. A solid black line at zero indicates no difference in SDV and serves as a reference for signal direction. See Figure 4B for a map of treated and untreated areas.

TABLE 4 **A summary of total water storage post-treatment 2023.**

Side of the ridge	Lidar-defined treated area (determined by ΔDCE; Figure 4B and Table 2)	Area (acre)	mm of SWE per m^2	Total water volume (acre-ft)	Difference (treated – untreated) (mm of SWE per m^2)	Difference in total water stored from treating the entire domain (acre-ft)	Potential difference in water stored per 100 acres of forest treatments (acre-ft)	
							Using a uniform snow density of 31%	Using field-based* densities of 34% (south) and 29% (north)
South	Untreated	24.4	94	7.5	15.4	1.2	5.1	5.6
	Treated	24.1	109	8.6				
North	Untreated	16.0	128	6.7	37.5	3.4	12.3	11.5
	Treated	27.7	165	15.0				

*The total water per 100 acres was calculated with variable snow densities of 34% on the south and 29% on the north, based on ground observations during the post-treatment lidar flight (Table 3).

the total area (Table 4). However, direct comparisons of total volume are limited because the two groups differ substantially in total area.

On the south side, a 15.4 mm SWE per m^2 difference yields a water storage benefit of 5.1 acre-feet per 100 acres of thinning, while on the north side, a 37.5 mm difference yields 12.3 acre-feet per 100 acres (Table 4). Accounting for field-based snow densities (Table 3), we find a change of +0.49 acre-feet on the south side and −0.8 acre-feet on the north side (Table 4). Even accounting for the potential for higher snow density on the south side, water storage gains are more than 2x greater on the north side.

4 Discussion

4.1 Synergy between fire fuels management and hydrologic resilience

We present the results of a before and after comparison of snowpack response to mechanical forest thinning on Cle Elum Ridge, in central Washington State. This area is characterized by dry mid-elevation forests that were historically adapted to frequent, low- or mixed-severity wildfires, with fire return intervals ranging from 7

to 40 years (Hessburg et al., 2005). Forests in this region have recently been subject to increasing levels of high-severity wildfire and drought, as well as a deficit of ecologically productive fire (Parks et al., 2025). While decades of previous studies have documented the effects of forest harvest on snow accumulation and water yield (e.g., Stednick, 1996; Troendle and Reuss, 1997), snow responses to forest management vary by climate, aspect, and management or disturbance (Dickerson-Lange et al., 2021; Gleason et al., 2019; Lundquist et al., 2013). These results provide a detailed look at snow response to a gradient of forest prescriptions across aspects in an actively managed forest landscape. Resilience to wildfire and climate change is a priority in the region, and managers are balancing community safety in the wildland-urban interface, working forest economies, water supplies, and vulnerable fish and wildlife habitat.

Our results show that fire fuel reduction strategies aimed at retaining individual trees, clumps, and openings (i.e., known as ICO approaches) used to recover fire-adapted forest patch structure and promote wildfire resilience in this region (Churchill et al., 2013; Hessburg et al., 2021) also promote hydrological resilience via increased snow storage. Compared to untreated forested areas, we observed greater water storage in canopy gaps between 4 and 16 m in diameter on both north- and south-facing slopes. We generally observed greater water storage benefits in gaps larger than 16 m in diameter than in forested areas, but interpreting large gap effects on snowpack is limited by a lack of sample size (i.e., few large gaps exist in the study domain). Water storage benefits resulting from thinning treatments were more than twice as great on north- versus south-facing slopes, yielding 12.3 versus 5.1 acre-feet of water per 100 acres of forest treatment, respectively.

These empirical observations are consistent with modeling results for the region. Modeled differences for peak SWE in the "wet/cold" climate of the Eastern Cascades (Sun et al., 2022) ranged from 10 to 60% between open areas and medium- or high-density forests. Watershed-scale modeling of forest thinning similarly found that forest treatments over a large spatial extent promote a moderate hydrologic buffering effect against climate-induced reductions in mountain snowpack (Furniss et al., 2025; Povak et al., 2022). However, fire fuel reduction and forest restoration strategies in this region and climate typically emphasize more intensive thinning on south-facing slopes. This study suggests that fire-fuel reduction and restoration to historical conditions may require reconsidering the treatment of north-facing slopes to better incorporate hydrologic resilience objectives.

The thinning project at Cle Elum Ridge represents a typical acreage for forest thinning activities. At this scale, water storage benefits support local soil moisture availability, increase forest resilience to drought, and contribute to in-stream flows in first- and second-order streams. Modeling results across similar geographies indicate that at least 50% of a watershed must be thinned to reliably increase streamflow at the HUC-12 scale (Furniss et al., 2025), a goal that has proven difficult to achieve in practice. Local-scale streamflow contributions, however, are potentially important for headwater stream ecosystems, which are especially sensitive to climate change (Leathers et al., 2024) and collectively responsible for 55% of the total river discharge exported from large river systems in the contiguous United States (Brinkerhoff et al., 2024). When paired with other strategies to support natural water storage functions to store and slow the export of water, such as restoring floodplain connectivity and shallow groundwater storage, upland water storage gains can support sensitive native fish populations dependent upon year-round water availability for rearing (Dittbrenner et al., 2022; Roni et al., 2015).

Furthermore, buffering climate impacts in snow-dominated river systems through forest treatments will likely be most beneficial during the early to mid-century (2020–2060), after which these areas will transition from snow- to rain-dominated systems (Vano et al., 2010). Both wildfire and mechanical treatments reduce forest density and help buffer declines in late spring and summer streamflow. Recent modeling efforts indicate that wildfire effects will eventually overshadow the results of mechanical thinning but also suggest that mechanical thinning treatments can be strategically used to increase the area burned and thereby improve the hydrological response in these historically fire-adapted landscapes. Thinning can also result in lower-severity burns that have less impact on snowpack duration and melt rate than high-severity burns (Koshkin et al., 2022).

Thus, while the long-term ability of mechanical thinning alone to buffer climate impacts on hydrology in this region is limited over the next four decades, thinning treatments provide both a near-term water storage benefit and a long-term mechanism to facilitate more ecologically positive fire. This approach also allows managers to let more fires burn while protecting communities and vulnerable ecosystems (Furniss et al., 2025).

4.2 Snow depth response relates to the arrangement of forest canopy rather than basal area

Our results suggest that sky view fraction is a dominant process in snow accumulation, whereas basal area is not. From a process perspective, snow interception and canopy shading are the primary controls on snow depth and duration on the north side of the ridge, and sky view fraction, but not basal area, reflects these processes. After treatments, snow depth increased most on the north side of the ridge in areas where the canopy transitioned from forest to fully open (Figure 7), which were also the areas with the greatest change in distance to the canopy edge (ΔDCE). In contrast, the nonlinear relationship between snow depth and sky view fraction on the south side of the ridge suggests that other physical processes dominate snow depth and duration for south-facing slopes (see Section 4.3).

From a forest management application perspective, these results highlight the need to consider traditional metrics, such as basal area, alongside canopy-focused metrics, such as canopy cover or DCE. The results demonstrate that for this site, the forest treatment stands, which represent a gradient of forest thinning from a basal area perspective, do not represent a similar gradient in DCE or percentage of canopy cover (Figures 6C–F). Since forest treatments create a combination of gaps and non-gaps that influence snow storage, quantifying canopy metrics is a necessary step for predicting the hydrologic response to forest treatments.

4.3 Future research

Differences in snow depth and duration between plots with similar forest structure and aspect on the south side of the ridge highlight the influence of ground cover and understory vegetation. In particular, the

CS-20 plot retains deeper snow and experiences later melt-out than all other south side plots (Figure 10A), despite being structurally similar to the CS-Gap plot. Both are located in canopy gaps with a single large tree, share similar aspects, and have comparable heat indices, yet snow at the CS-20 plot persists for more than 20 days longer and is twice as deep as at the CS-Gap plot. While the sky view fraction partially explains snowpack variability on the north side of the ridge (Figure 5D), it does not fully account for the differences between the two south side plots (Figure 5C and Figure 10B).

Time-lapse photos suggest that ground cover may be a key differentiator. The CS-20 plot has minimal understory vegetation beneath the canopy (Figure 10D), whereas the CS-Gap plot is densely populated with shrubs 1–2 m tall (Figure 10C). Given that snow depths are often <1 m on the south side of the ridge, this vegetation remains exposed for much of the winter, absorbing solar radiation. While tree trunks absorb heat and emit longwave radiation to melt the surrounding snowpack, they also provide vital shading from shortwave radiation on slopes with high radiative heating (Webster et al., 2016). Similarly, understory vegetation can heat up and melt the surrounding snowpack (Pomeroy et al., 2009), without providing the same shading benefits as the forest canopy. Additionally, the resulting patchy snow cover can further enhance snowmelt through turbulent fluxes (Haugeneder et al., 2024).

Thus, our results suggest that removing understory vegetation and vegetation within gaps might maximize snow retention in areas with high radiative heating. While additional research is needed on the effects of prescribed burns on snow depth (Koshkin et al., 2022), forest management practices that remove understory vegetation (e.g., prescribed fire, shrub removal, and mastication) may positively affect snow depth and retention in a changing climate. Historically, fire intervals in this region ranged from 7 to 40 years, which would have reset ground cover vegetation at recurring intervals. Identifying practical and effective return intervals for understory vegetation management in the context of wildfire resilience is a complex management task that requires integrating historical fire regimes, vegetation regrowth rates, management objectives, and site-specific conditions (Peterson et al., 2025). Our data indicate that future work should also explicitly consider the roles of ground-level forest fuels and management intervals in snow depth responses.

The response of snow depth to forest structure showed that gap size strongly influenced snow accumulation. On the south side of the ridge, the shallowest snowpack occurred in dense and sparse forest, while the deepest snowpack occurred in small and large gaps (Figures 8A,D). On the north side, snow depth peaked in these small gaps (4 to 16 m in diameter), with less accumulation in the large gaps (>16 m in diameter; Figures 8C,F). We urge caution with this result, given the limited sample size and the exposed, low-angle location of the existing large gaps within the study domain. Since the forest is primarily composed of tree clusters and small gaps (Figures 8B,E), our findings do not indicate how clear-cutting or creating larger openings would affect snow depth. We therefore caution against overly large

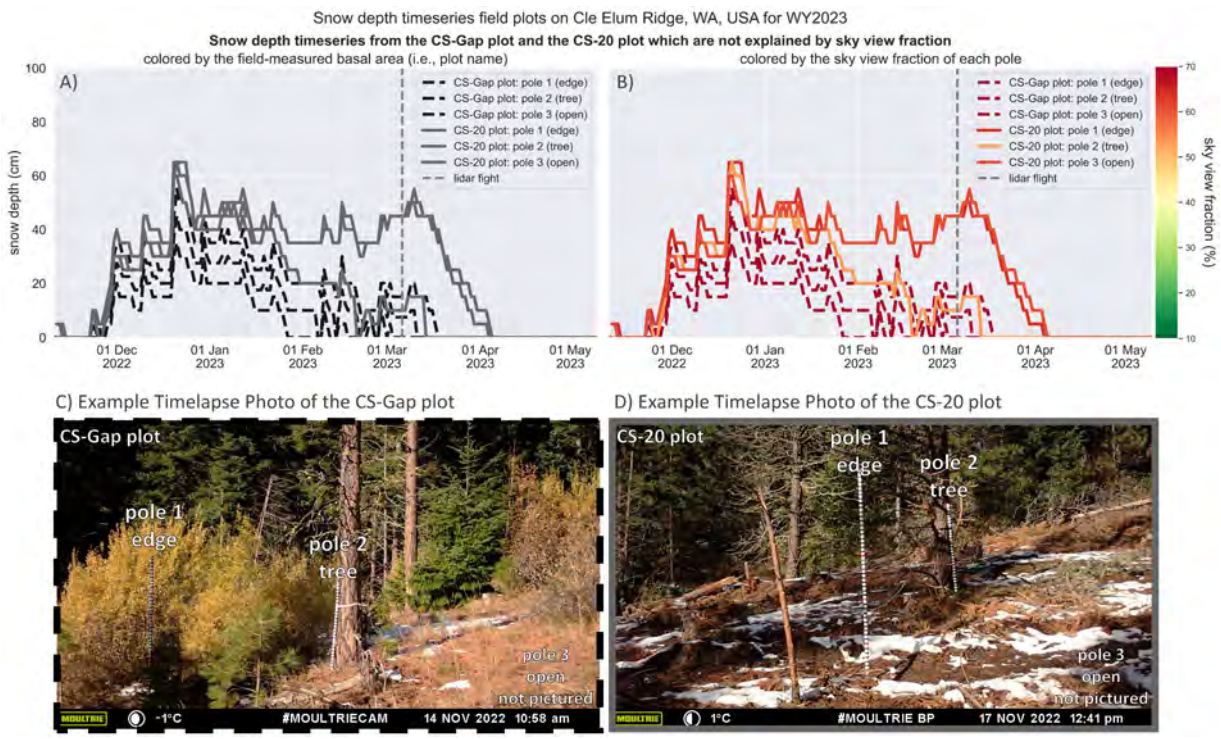

FIGURE 10
Snow depth (cm) timeseries from WY2023 for three poles in each plot, the CS-Gap and CS-20 plots, shown in two ways: **(A)** poles colored by plot name, reflecting the prescribed basal area, and **(B)** the same poles colored by their individual sky view fraction (%). While at other timeseries sites, snow depth patterns align with sky view fraction, they do not at poles 1 and 2 in the CS-20 plot. Example time-lapse photos of **(C)** the CS-Gap plot and **(D)** the CS-20 plot reveal contrasting ground cover—dense shrubs in CS-Gap and minimal understory in CS-20—which may explain the observed differences in snow depth despite similar sky view fractions.

gaps opened during forest thinning and suggest further research to optimize gap size for wildfire and hydrologic resilience.

Finally, Cle Elum Ridge shares forest and snow-climate characteristics with many mid-elevation managed forests across the western United States and globally (e.g., Dickerson-Lange et al., 2021). Future studies should assess how these forest-snow interactions vary across forest types and elevation gradients, especially as warming shifts snowpack thresholds upward and alters forest structure. Understanding these dynamics will be essential for optimizing forest management to support both snow retention and ecosystem resilience.

5 Conclusion

We found that experimental forest treatments designed to reduce wildfire risk also increased overall snow storage, with the largest positive influence on north-facing slopes and in small- to medium-sized gaps. Thinning treatments thus provide a synergistic response between wildfire and hydrologic resilience in the dry forests of the Eastern Cascades Range in Washington State, USA. With respect to bridging forest practice metrics and snow hydrology metrics, we found that the basal area metric used by foresters to prescribe thinning treatment levels did not directly correspond to the factors that influence snow depth, and that landscape managers may need to incorporate metrics such as distance to canopy edge and sky view fraction into their planning efforts. Thus, rather than identifying basal area targets to optimize snow retention, we recommend creating gaps between 4 and 16 m in diameter to enhance snow retention. This aligns with current forest restoration recommendations for this region, which aim to restore historical patch structure and fire regimes (Hessburg et al., 2021). Our data further show that creating canopy gaps on north-facing slopes will confer the greatest hydrologic benefit. Due to the lack of gaps larger than 16 m in diameter at our site, we emphasize the need for additional research to determine the impact of larger gaps on snow retention in this region. We observed similar, but more muted, patterns in the shallower snowpack on the south-facing slopes of Cle Elum Ridge, which had a comparatively sparse forest structure prior to forest treatments. Time-lapse photography suggests that ground vegetation plays a larger role in snow depth than overall forest structure in areas with high radiative heating in this region. Thus, we emphasize the need for further research on how forest management practices to remove understory vegetation, such as mastication, prescribed burns, and shrub removal, influence snow depth on slopes with high radiative heating. Additionally, the climatic characteristics and forest-snow interactions at Cle Elum Ridge are likely similar to numerous managed forests across the western USA (e.g., Figure 3; Dickerson-Lange et al., 2021) and the world, and future work should explore how these findings vary across forest types and elevations, particularly in the context of climate change.

Data availability statement

The data presented in the study are deposited in the HydroShare repository, accession number 10.4211/hs.96f4199c0e4c48e6bc0ea7f9251b16dd. The HydroShare repository includes all datasets required to reproduce the analyses and figures presented in this study. All code used to reproduce the analyses and figures is publicly available at https://github.com/cassielumbrazo/CER_treatment_manuscript.

Author contributions

CL: Data curation, Formal analysis, Methodology, Visualization, Writing – original draft, Writing – review & editing. EH: Conceptualization, Funding acquisition, Methodology, Project administration, Resources, Supervision, Writing – original draft, Writing – review & editing. SD-L: Conceptualization, Formal analysis, Funding acquisition, Methodology, Supervision, Visualization, Writing – original draft, Writing – review & editing. SP: Formal analysis, Methodology, Visualization, Writing – review & editing. JC: Data curation, Visualization, Writing – original draft. KD: Data curation, Resources, Writing – review & editing. KS: Methodology, Resources, Writing – review & editing. JL: Conceptualization, Funding acquisition, Project administration, Resources, Supervision, Writing – review & editing.

Funding

The author(s) declared that financial support was received for this work and/or its publication. The Washington Department of Natural Resources (DNR) provided funding through interagency agreement number 93-104079. The Nature Conservancy provided funding through TNC WA-G-220620-026. Data was collected in part using equipment provided by the National Science Foundation as part of the RAPID Facility, a component of the Natural Hazards Engineering Research Infrastructure, under award no. CMMI: 2130997. Any opinions, findings, conclusions, and recommendations presented in this paper are those of the author(s) and do not necessarily reflect the views of the funding entities.

Acknowledgments

Herman Flamenco, at The Nature Conservancy, led the implementation of forest thinning treatments at the study site. The author(s) would like to thank The Nature Conservancy team and Herman for stewarding this land, for his support with field logistics, and for his unwavering patience with our many questions about methods and locations. Iron Mountain Lumber Co., owner and operator, Rob Deter and crew, was the contract logger who completed the thinning treatments and assisted the forest managers in implementing the project. Connor Craig and the Wildfire Home Protection crew completed mastication within the treatment areas. The author(s) would like to thank the Tapash Sustainable Forest Collaborative's executive team for their conversations that led to the development of this project. Members represent the Confederated Tribes and Bands of the Yakama Nation, The Nature Conservancy, the USDA Forest Service, the Washington Department of Fish and Wildlife, and the Washington State Department of Natural Resources. The author(s) would also like to thank the RAPID Field Team, who helped collect the post-treatment lidar; Andrew Lyda, Michael Grilliot, and Jaqueline Zdebski; and others who joined on the ridge to help with fieldwork: Mari Cleven, Mark Stone, and Mackenzie Stuart. We are grateful to Max Lambert for helpful comments on an earlier draft of this manuscript. The graphical

abstract of this manuscript includes a drone photograph of the ridge taken by Mark Stone, along with adapted illustrations from the Integration and Application Network at the University of Maryland Center for Environmental Science (UMCES), used under the Creative Commons Attribution-ShareAlike 4.0 International License (CC BY-SA 4.0). The original illustrations are by Lucy Van Essen-Fishman (*Pinus ponderosa*), Jane Hawkey (*Pinus palustris*), Kim Kraeer (*Pinus ponderosa*), Kate Moore (*logging*), Emily Nastase (*Juniperus monosperma*), and Tracy Saxby (*Pinus glauca* and *shrubs*). The author(s) thank the handling editor and the two reviewers for their thoughtful and constructive comments, which greatly improved the quality and clarity of this manuscript.

Conflict of interest

The author(s) declared that this work was conducted in the absence of any commercial or financial relationships that could be construed as a potential conflict of interest.

Generative AI statement

The author(s) declared that Generative AI was not used in the creation of this manuscript.

Any alternative text (alt text) provided alongside figures in this article has been generated by Frontiers with the support of artificial intelligence and reasonable efforts have been made to ensure accuracy, including review by the author(s) wherever possible. If you identify any issues, please contact us.

Publisher's note

References

Abatzoglou, J. T., Battisti, D. S., Williams, A. P., Hansen, W. D., Harvey, B. J., and Kolden, C. A. (2021). Projected increases in western US forest fire despite growing fuel constraints. *Commun. Earth Environ.* 2:227. doi: 10.1038/s43247-021-00299-0

Abatzoglou, J. T., and Williams, A. P. (2016). Impact of anthropogenic climate change on wildfire across western US forests. *Proc. Natl. Acad. Sci. USA* 113, 11770–11775. doi: 10.1073/pnas.1607171113

Abatzoglou, J. T., Williams, A. P., Boschetti, L., Zubkova, M., and Kolden, C. A. (2018). Global patterns of interannual climate–fire relationships. *Glob. Chang. Biol.* 24, 5164–5175. doi: 10.1111/gcb.14405

Bales, R. C., Hopmans, J. W., O'Geen, A. T., Meadows, M., Hartsough, P. C., Kirchner, P., et al. (2011). Soil moisture response to snowmelt and rainfall in a Sierra Nevada mixed-conifer forest. *Vadose Zone J.* 10, 786–799. doi: 10.2136/vzj2011.0001

Berman, J. W., Wartman, J., Olsen, M., Irish, J. L., Miles, S. B., Tanner, T., et al. (2020). Natural hazards reconnaissance with the NHERI RAPID facility. *Front. Built Environ.* 6:67. doi: 10.3389/fbuil.2020.573067

Brinkerhoff, C. B., Gleason, C. J., Kotchen, M. J., Kysar, D. A., and Raymond, P. A. (2024). Ephemeral stream water contributions to United States drainage networks. *Science* 384, 1476–1482. doi: 10.1126/science.adg9430

Brown, T. C., Mahat, V., and Ramirez, J. A. (2019). Adaptation to future water shortages in the United States caused by population growth and climate change. *Earth's Future* 7, 219–234. doi: 10.1029/2018EF001091

Churchill, D., Jeronimo, S., Larson, A., Fischer, P., Dahlgreen, M., and Franklin, J. (2016). The ICO approach to quantifying and restoring Forest spatial pattern: implementation guide. ICO App. Available online at: https://scholarworks.umt.edu/ico/3 (Accessed January 10, 2023).

Churchill, D. J., Larson, A. J., Dahlgreen, M. C., Franklin, J. F., Hessburg, P. F., and Lutz, J. A. (2013). Restoring forest resilience: from reference spatial patterns to silvicultural prescriptions and monitoring. *For. Ecol. Manag.* 291, 442–457. doi: 10.1016/j.foreco.2012.11.007

Cline, T. J., Schindler, D. E., Walsworth, T. E., French, D. W., and Lisi, P. J. (2020). Low snowpack reduces thermal response diversity among streams across a landscape. *Limnol. Oceanogr. Lett.* 5, 254–263. doi: 10.1002/lol2.10148

Cristea, N. C., Breckheimer, I., Raleigh, M. S., HilleRisLambers, J., and Lundquist, J. D. (2017). An evaluation of terrain-based downscaling of fractional snow covered area data sets based on LiDAR-derived snow data and orthoimagery. *Water Resour. Res.* 53, 6802–6820. doi: 10.1002/2017WR020799

Dickerson-Lange, S. E., Gersonde, R. F., Hubbart, J. A., Link, T. E., Nolin, A. W., Perry, G. H., et al. (2017). Snow disappearance timing is dominated by forest effects on snow accumulation in warm winter climates of the Pacific northwest, United States. *Hydrol. Process.* 31, 1846–1862. doi: 10.1002/hyp.11144

Dickerson-Lange, S. E., Howe, E. R., Patrick, K., Gersonde, R., and Lundquist, J. D. (2023). Forest gap effects on snow storage in the transitional climate of the eastern Cascade Range, Washington, United States. *Front. Water* 5:5264. doi: 10.3389/frwa.2023.1115264

Dickerson-Lange, S. E., Lutz, J. A., Gersonde, R., Martin, K. A., Forsyth, J. E., and Lundquist, J. D. (2015). Observations of distributed snow depth and snow duration within diverse forest structures in a maritime mountain watershed. *Water Resour. Res.* 51, 9353–9366. doi: 10.1002/2015WR017873

Dickerson-Lange, S. E., Vano, J. A., Gersonde, R., and Lundquist, J. D. (2021). Ranking forest effects on snow storage: a decision tool for forest management. *Water Resour. Res.* 57:e2020WR027926. doi: 10.1029/2020WR027926

Dittbrenner, B. J., Schilling, J. W., Torgersen, C. E., and Lawler, J. J. (2022). Relocated beaver can increase water storage and decrease stream temperature in headwater streams. *Ecosphere* 13:e4168. doi: 10.1002/ecs2.4168

Donley, E. E., Naiman, R. J., and Marineau, M. D. (2012). Strategic planning for instream flow restoration: a case study of potential climate change impacts in the Central Columbia River basin. *Glob. Chang. Biol.* 18, 3071–3086. doi: 10.1111/j.1365-2486.2012.02773.x

Duan, K., Sun, G., McNulty, S. G., Caldwell, P. V., Cohen, E. C., Sun, S., et al. (2017). Future shift of the relative roles of precipitation and temperature in controlling annual runoff in the conterminous United States. *Hydrol. Earth Syst. Sci.* 21, 5517–5529. doi: 10.5194/hess-21-5517-2017

Elledge, J., and Barlow, B. (2018). Basal area: a measure made for management Alabama cooperative extension system. Available online at: https://www.aces.edu/blog/topics/forestry/basal-area-a-measure-made-for-management/ (Accessed September 5, 2025).

Everett, R. L., Schellhaas, R., Keenum, D., Spurbeck, D., and Ohlson, P. (2000). Fire history in the ponderosa pine/Douglas-fir forests on the east slope of the Washington cascades. *For. Ecol. Manag.* 129, 207–225. doi: 10.1016/S0378-1127(99)00168-1

Furniss, T. J., Hessburg, P. F., Churchill, D., Wigmosta, M., Povak, N., Duan, Z., et al. (2025). Wildfire and forest treatments mitigate—but cannot forestall—climate-driven changes in streamflow regimes in a western US mountain landscape. *Environ. Res. Lett.* 20:084039. doi: 10.1088/1748-9326/ade896

Gelfan, A. N., Pomeroy, J. W., and Kuchment, L. S. (2004). Modeling forest cover influences on snow accumulation, sublimation, and melt. *J. Hydrometeorol.* 5, 785–803. doi: 10.1175/1525-7541(2004)005%3C0785:MFCIOS%3E2.0.CO;2

Gergel, D. R., Nijssen, B., Abatzoglou, J. T., Lettenmaier, D. P., and Stumbaugh, M. R. (2017). Effects of climate change on snowpack and fire potential in the western USA. *Clim. Chang.* 141, 287–299. doi: 10.1007/s10584-017-1899-y

Gleason, A. (2018). Yakima Basin North LiDAR report [technical data report] quantum spatial (QSI). Available online at: https://www.fisheries.noaa.gov/inport/item/67534 (Accessed June 1, 2022).

Gleason, K. E., McConnell, J. R., Arienzo, M. M., Chellman, N., and Calvin, W. M. (2019). Four-fold increase in solar forcing on snow in western U.S. burned forests since 1999. *Nat. Commun.* 10:2026. doi: 10.1038/s41467-019-09935-y

Hagmann, R. K., Hessburg, P. F., Prichard, S. J., Povak, N. A., Brown, P. M., Fulé, P. Z., et al. (2021). Evidence for widespread changes in the structure, composition, and fire regimes of western North American forests. *Ecol. Appl.* 31:e02431. doi: 10.1002/eap.2431

Halofsky, J. E., Peterson, D. L., and Harvey, B. J. (2020). Changing wildfire, changing forests: the effects of climate change on fire regimes and vegetation in the Pacific northwest, USA. *Fire Ecol.* 16:4. doi: 10.1186/s42408-019-0062-8

Harrod, R. J., McRae, B. H., and Hartl, W. E. (1999). Historical stand reconstruction in ponderosa pine forests to guide silvicultural prescriptions. *For. Ecol. Manag.* 114, 433–446. doi: 10.1016/S0378-1127(98)00373-9

Haugeneder, M., Lehning, M., Stiperski, I., Reynolds, D., and Mott, R. (2024). Turbulence in the strongly heterogeneous near-surface boundary layer over patchy snow. *Boundary-Layer Meteorol.* 190:7. doi: 10.1007/s10546-023-00856-4

Hessburg, P. F., Agee, J. K., and Franklin, J. F. (2005). Dry forests and wildland fires of the inland Northwest USA: contrasting the landscape ecology of the pre-settlement and modern eras. *For. Ecol. Manag.* 211, 117–139. doi: 10.1016/j.foreco.2005.02.016

Hessburg, P. F., Prichard, S. J., Hagmann, R. K., Povak, N. A., and Lake, F. K. (2021). Wildfire and climate change adaptation of western North American forests: a case for intentional management. *Ecol. Appl.* 31:e02432. doi: 10.1002/eap.2432

Koivusalo, H., and Kokkonen, T. (2002). Snow processes in a forest clearing and in a coniferous forest. *J. Hydrol.* 262, 145–164. doi: 10.1016/S0022-1694(02)00031-8

Koshkin, A. L., Hatchett, B. J., and Nolin, A. W. (2022). Wildfire impacts on western United States snowpacks. *Front. Water* 4:1271. doi: 10.3389/frwa.2022.971271

Leathers, K., Herbst, D., de Mendoza, G., Doerschlag, G., and Ruhi, A. (2024). Climate change is poised to alter mountain stream ecosystem processes via organismal phenological shifts. *Proc. Natl. Acad. Sci.* 121:e2310513121. doi: 10.1073/pnas.2310513121

Li, D., Wrzesien, M. L., Durand, M., Adam, J., and Lettenmaier, D. P. (2017). How much runoff originates as snow in the western United States, and how will that change in the future? *Geophys. Res. Lett.* 44, 6163–6172. doi: 10.1002/2017GL073551

Lumbrazo, C. (2021). Hydrologic effects of Forest restoration, WA 2021. [airborne Lidar]. San Diego, CA, USA: OpenTopography, National Center for Airborne Laser Mapping (NCALM). doi: 10.5069/G989142F

Lumbrazo, C., Dedinsky, K., Lyda, A., Grilliot, M., and Zdebski, J. (2025). Cle Elum Ridge snow-on lidar for forest management [dataset]. Austin, TX, USA: DesignSafe-CI, Texas Advanced Computing Center (TACC). doi: 10.17603/ds2-8hz4-zb88

Lundquist, J. D., Dickerson-Lange, S. E., Lutz, J. A., and Cristea, N. C. (2013). Lower forest density enhances snow retention in regions with warmer winters: a global framework developed from plot-scale observations and modeling. *Water Resour. Res.* 49, 6356–6370. doi: 10.1002/wrcr.20504

Manning, A., Csank, A., Allen, S., and Harpold, A. (2025). Differential snow depth in warm edges versus cold edges of forest gaps, and its potential implications for tree growth in a sierra Nevada conifer forest. *For. Ecol. Manag.* 597:123119. doi: 10.1016/j.foreco.2025.123119

Mazzotti, G., Currier, W. R., Deems, J. S., Pflug, J. M., Lundquist, J. D., and Jonas, T. (2019). Revisiting snow cover variability and canopy structure within forest stands: insights from airborne lidar data. *Water Resour. Res.* 55, 6198–6216. doi: 10.1029/2019WR024898

Mote, P. W., Hamlet, A. F., Clark, M. P., and Lettenmaier, D. P. (2005). Declining mountain snowpack in Western North America. *Bull. Am. Meteorol. Soc.* 86, 39–50. doi: 10.1175/BAMS-86-1-39

Mote, P. W., Li, S., Lettenmaier, D. P., Xiao, M., and Engel, R. (2018). Dramatic declines in snowpack in the western US. *NPJ Clim. Atmos. Sci.* 1:1. doi: 10.1038/s41612-018-0012-1

Musselman, K. N., Clark, M. P., Liu, C., Ikeda, K., and Rasmussen, R. (2017). Slower snowmelt in a warmer world. *Nat. Clim. Chang.* 7:3. doi: 10.1038/nclimate3225

Musselman, K. N., Lehner, F., Ikeda, K., Clark, M. P., Prein, A. F., Liu, C., et al. (2018). Projected increases and shifts in rain-on-snow flood risk over western North America. Nature. *Climate Change* 8, 808–812. doi: 10.1038/s41558-018-0236-4

Newton, B., and Spence, C. (2023). JAMES BUTTLE review: a resilience framework for physical hydrology. *Hydrol. Process.* 37:e14926. doi: 10.1002/hyp.14926

Norton, A. (2015). Teanaway community Forest LiDAR report [technical data report] quantum spatial (QSI). Available online at: pugetsoundlidar.ess.washington.edu/lidardata/proj_reports/PLSC_Teanaway_Community_Forest_LiDAR_Report.pdf (Accessed June 3, 2022).

Parks, S. A., Guiterman, C. H., Margolis, E. Q., Lonergan, M., Whitman, E., Abatzoglou, J. T., et al. (2025). A fire deficit persists across diverse North American forests despite recent increases in area burned. *Nat. Commun.* 16:1493. doi: 10.1038/s41467-025-56333-8

Peterson, D. W., Harrod, R. J., Dodson, E. K., Ohlson, P. L., Pawlikowski, N. C., Ireland, K. B., et al. (2025). Mechanical mastication and prescribed burning reduce forest fuels and alter stand structure in dry coniferous forests. *For. Ecol. Manag.* 593:122909. doi: 10.1016/j.foreco.2025.122909

Pflug, J. M., and Lundquist, J. D. (2020). Inferring distributed snow depth by leveraging snow pattern repeatability: investigation using 47 Lidar observations in the Tuolumne watershed, Sierra Nevada, California. *Water Resour. Res.* 56:e2020WR027243. doi: 10.1029/2020WR027243

Pierce, D. W., Barnett, T. P., Hidalgo, H. G., Das, T., Bonfils, C., Santer, B. D., et al. (2008). Attribution of declining Western U.S. snowpack to human effects. *J. Clim.* 21, 6425–6444. doi: 10.1175/2008JCLI2405.1

Pomeroy, J. W., Marks, D., Link, T., Ellis, C., Hardy, J., Rowlands, A., et al. (2009). The impact of coniferous forest temperature on incoming longwave radiation to melting snow. *Hydrol. Process.* 23, 2513–2525. doi: 10.1002/hyp.7325

Povak, N. A., Furniss, T. J., Hessburg, P. F., Salter, R. B., Wigmosta, M., Duan, Z., et al. (2022). Evaluating basin-scale Forest adaptation scenarios: wildfire, streamflow, biomass, and economic recovery synergies and trade-offs. *Front. For. Glob. Change* 5:5179. doi: 10.3389/ffgc.2022.805179

Prichard, S. J., Hessburg, P. F., Hagmann, R. K., Povak, N. A., Dobrowski, S. Z., Hurteau, M. D., et al. (2021). Adapting western North American forests to climate change and wildfires: 10 common questions. *Ecol. Appl.* 31:e02433. doi: 10.1002/eap.2433

Richards, D. (2014). Timber cruising handbook. Washington State Department of Natural Resources. Available online at: dnr.wa.gov/sites/default/files/2025-05/psl_ts_cruisinghandbook.pdf (Accessed April 19, 2023).

Roni, P., Beechie, T., Pess, G., and Hanson, K. (2015). Wood placement in river restoration: fact, fiction, and future direction. *Can. J. Fish. Aquat. Sci.* 72, 466–478. doi: 10.1139/cjfas-2014-0344

Rutter, N., Essery, R., Pomeroy, J., Altimir, N., Andreadis, K., Baker, I., et al. (2009). Evaluation of forest snow processes models (SnowMIP2). *J. Geophys. Res. Atmos.* 114:1063. doi: 10.1029/2008JD011063

Sanmiguel-Vallelado, A., McPhee, J., Esmeralda Ojeda Carreño, P., Morán-Tejeda, E., Julio Camarero, J., and López-Moreno, J. I. (2022). Sensitivity of forest–snow interactions to climate forcing: local variability in a Pyrenean valley. *J. Hydrol.* 605:127311. doi: 10.1016/j.jhydrol.2021.127311

SilviaTerra (2017). Plot hound (version 1) [computer software] southern regional extension forestry. Available online at: https://sref.info/resources/mobile-apps/plot-hound (Accessed March 22, 2021).

Stednick, J. D. (1996). Monitoring the effects of timber harvest on annual water yield. *J. Hydrol.* 176, 79–95. doi: 10.1016/0022-1694(95)02780-7

Storck, P. (2000). Trees, snow, and flooding: An investigation of forest canopy effects on snow accumulation and melt at the plot and watershed scales in the Pacific Northwest [Ph.D., University of Washington]. Seattle, WA, USA: University of Washington.

Sturm, M., and Wagner, A. M. (2010). Using repeated patterns in snow distribution modeling: an Arctic example. *Water Resour. Res.* 46:9434. doi: 10.1029/2010WR009434

Sun, N., Yan, H., Wigmosta, M. S., Lundquist, J., Dickerson-Lange, S., and Zhou, T. (2022). Forest canopy density effects on snowpack across the climate gradients of the Western United States Mountain ranges. *Water Resour. Res.* 58:e2020WR029194. doi: 10.1029/2020WR029194

Troendle, C. A., and Reuss, J. O. (1997). Effect of clear cutting on snow accumulation and water outflow at Fraser, Colorado. *Hydrol. Earth Syst. Sci.* 1, 325–332. doi: 10.5194/hess-1-325-1997

U.S. Bureau of Reclamation (USBR) (2002). Interim comprehensive basin operating plan. Washington: Yakima Project.

Vano, J. A., Scott, M. J., Voisin, N., Stöckle, C. O., Hamlet, A. F., Mickelson, K. E. B., et al. (2010). Climate change impacts on water management and irrigated agriculture in the Yakima River basin, Washington, USA. *Clim. Chang.* 102, 287–317. doi: 10.1007/s10584-010-9856-z

Wartman, J., Berman, J. W., Bostrom, A., Miles, S., Olsen, M., Gurley, K., et al. (2020). Research needs, challenges, and strategic approaches for natural hazards and disaster reconnaissance. *Front. Built Environ.* 6:3068. doi: 10.3389/fbuil.2020.573068

Washington Geological Survey (2015) Teanaway LiDAR 2015 [LiDAR data] Washington Dept. of Natural Resources (WA DNR) LiDAR portal. Available online at: https://lidarportal.dnr.wa.gov/ (Accessed May 2, 2022).

Washington Geological Survey. (2018). Yakima Basin North LiDAR 2018 (LiDAR data no. contracted via quantum spatial (QSI)). Washington Dept. of natural resources (WA DNR) LiDAR Portal. Available online at: https://lidarportal.dnr.wa.gov/ (Accessed May 2, 2022).

Washington State Department of Natural Resources. 2018a. 20-year Forest health strategic plan—Eastern Washington planning area prioritization Washington State Department of Natural Resources. Available online at: https://dnr.wa.gov/sites/default/files/2025-03/rp_forest_health_20_year_strategic_plan.pdf (Accessed February 20, 2022).

Washington State Department of Natural Resources. (2018b). Forest health assessment and treatment framework (SB 5546) (p. 66) [Report to the Legislature]. Washington State Department of Natural Resources. Available online at: https://dnr.wa.gov/sites/default/files/2025-05/rp_2018_forest_health_assessment_treatment_framework_report.pdf (Accessed February 10, 2022).

Webster, C., Rutter, N., Zahner, F., and Jonas, T. (2016). Measurement of incoming radiation below forest canopies: a comparison of different radiometer configurations. *J. Hydrometeorol.* 17, 853–864. doi: 10.1175/JHM-D-15-0125.1

Weinberger, H. (2022). Billions of federal dollars headed to Western forests to manage fires | Cascade PBS. CASCADE PBS Environment. Available online at: https://www.cascadepbs.org/environment/2022/02/billions-federal-dollars-headed-western-forests-manage-fires (Accessed September 28, 2023).

Western Region Climate Center (WRCC) (2007). Monthly climate summaries. Available online at: https://wrcc.dri.edu/summary/Climsmwa.html (Accessed September 18, 2022).

Wright, C. S., and Agee, J. K. (2004). Fire and vegetation history in the eastern Cascade Mountains, Washington. *Ecol. Appl.* 14, 443–459. doi: 10.1890/02-5349